

MMOTU: A Multi-Modality Ovarian Tumor Ultrasound Image Dataset for Unsupervised Cross-Domain Semantic Segmentation

Qi Zhao^{a,1}, Shuchang Lyu^{a,1}, Wenpei Bai^{b,1}, Linghan Cai^{a,1}, Binghao Liu^a, Guangliang Cheng^c, Meijing Wu^b, Xiubo Sang^b, Min Yang^{b,**} and Lijiang Chen^{a,*}

^aDepartment of Electronics and Information Engineering, Beihang University, Xueyuan Road No.37, Haidian district, Beijing, 100191, China

^bDepartment of Gynecology and Obstetrics, Beijing Shijitan Hospital, Capital Medical University, Tieyi Road No.10, Haidian district, Beijing, 100038, China

^cUniversity of Liverpool, Foundation Building, Brownlow Hill,, Liverpool, L693BX, , UK

ARTICLE INFO

Keywords:

Ovarian tumor ultrasound image dataset
Multi-Modality feature representation
Cross-domain semantic segmentation
Dual-scheme domain-selected network
Unsupervised Domain Adaptation

ABSTRACT

Ovarian cancer is one of the most harmful gynecological diseases. Detecting ovarian tumors in early stage with computer-aided techniques can efficiently decrease the mortality rate. With the improvement of medical treatment standard, ultrasound images are widely applied in clinical treatment. However, recent notable methods mainly focus on single-modality ultrasound ovarian tumor segmentation or recognition, which means there still lacks researches on exploring the representation capability of multi-modality ultrasound ovarian tumor images. To solve this problem, we propose a Multi-Modality Ovarian Tumor Ultrasound (MMOTU) image dataset containing 1469 2d ultrasound images and 170 contrast enhanced ultrasonography (CEUS) images with pixel-wise and global-wise annotations. Based on MMOTU, we mainly focus on unsupervised cross-domain semantic segmentation task. To solve the domain shift problem, we propose a feature alignment based architecture named Dual-Scheme Domain-Selected Network (DS²Net). Specifically, we first design source-encoder and target-encoder to extract two-style features of source and target images. Then, we propose Domain-Distinct Selected Module (DDSM) and Domain-Universal Selected Module (DUSM) to represent the distinct and universal features in two styles (source-style or target-style). Finally, we fuse these two kinds of features and feed them into the source-decoder and target-decoder to generate final predictions. Extensive comparison experiments and analysis on MMOTU image dataset show that DS²Net can boost the segmentation performance for bidirectional cross-domain adaptation of 2d ultrasound and CEUS images. Our proposed dataset and code are all available at https://github.com/cv516Buua/MMOTU_DS2Net.

1. Introduction

Ovarian cancer is one of the most mortal gynecological diseases, which ranks 8th among all the gynecological cancers Siegel et al. (2021). Diagnosing and detecting ovarian tumors in the early stage can significantly decrease the mortality rate. At present, the common-used screening techniques are two-dimensional (2d) ultrasound scanning, contrast enhanced ultrasonography (CEUS), Computed Tomography (CT) and Magnetic Resonance Imaging (MRI). Among them, 2d ultrasound scanning is the most widely-applied technique, because it is more convenient and has less impact on human body.

Recently, several methods focus on computer-aided detecting and diagnosing ovarian tumors Wu et al. (2018); Wang and Zeng (2021); Yang et al. (2021); Qian et al. (2022); Li et al. (2020); Wu et al. (2023). Despite their notable works, there still exists the following two main

weaknesses. First, recent methods only focus on single-modality segmentation and recognition (mainly on 2d ultrasound images). There still lacks researches on exploring the representation potential of multi-modality ultrasound images because of lacking standard datasets. Second, even though many notable methods Tsai et al. (2018); Hoffman et al. (2018); Zhu et al. (2017); Chen et al. (2020); Zou et al. (2020) make huge progress on cross-domain adaptation, there still lacks solution on tackling cross-domain segmentation among multi-modality ultrasound images.

To solve the above-mentioned two weaknesses, we first construct a Multi-Modality Ovarian Tumor Ultrasound (MMOTU) image dataset. MMOTU image dataset consists of two sub-sets with two modalities, which respectively contain 1469 2d ultrasound images (OTU_2d) and 170 CEUS images (OTU_CEUS). On these two sub-sets, we provide pixel-wise semantic annotations and global-wise category annotations. Then, we explore the cross-domain representation potential on MMOTU image dataset. As shown in Fig.1, we tackle three tasks on MMOTU image dataset. The second task (unsupervised domain adaptation based semantic segmentation) is our main research focus, which aims to boost the segmentation performance on target samples with only source annotated samples for training. The first task (semantic segmentation) is the prior research of second task. The third task (recognition task) is also meaningful for clinical treatment.

*Primary Corresponding author

**Secondary Corresponding author

✉ zhaoqi@buaa.edu.cn (Q. Zhao); lyushuchang@buaa.edu.cn (S. Lyu); baiwp@bjsjth.cn (W. Bai); cai1h@buaa.edu.cn (L. Cai); liubinghao@buaa.edu.cn (B. Liu); Guangliang.Cheng@liverpool.ac.uk (G. Cheng); nancywu0429@foxmail.com (M. Wu); sangxiubo3506@bjsjth.cn (X. Sang); yangmin@bjsjth.cn (M. Yang); chenlijiang@buaa.edu.cn (L. Chen)
ORCID(s): 0000-0001-9769-7083 (S. Lyu)

¹Contribute Equally.

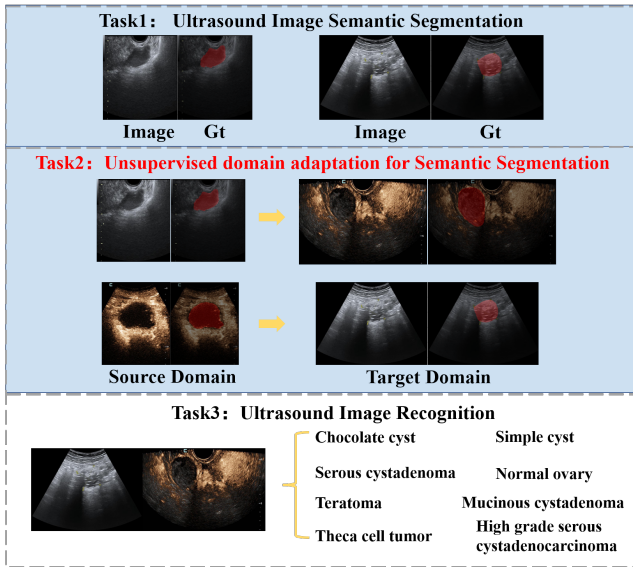


Figure 1: Task description on MMOTU image dataset. **Task1:** single-modality semantic segmentation. **Task2:** bidirectional unsupervised domain adaptation between OTU_2d and OTU_CEUS for semantic segmentation. **Task3:** single-modality image recognition. Here, Task2 is our main research focus. Task1 is the prior research of Task2. Task3 is an independent task, which is also meaningful in clinical treatment.

Recently, deep convolutional neural networks (DCNNs) have shown great success on recognition Chi et al. (2017); Wang et al. (2021); Zhang et al. (2019); Zhu et al. (2021); He et al. (2021); Wu et al. (2018) and semantic segmentation Ronneberger et al. (2015); Chen et al. (2021); Zhou et al. (2018); Zhang et al. (2021) of medical images. These two tasks play an important role on computer-aided clinical diagnosis. Based on MMOTU image dataset, we first tackle single-modality semantic segmentation task, which aims to find the lesion region. In clinical treatment, this task can apply on computing the measurements. We typically hope to report tumor size using segmentation result as prior knowledge. This task also provides evidence for recognition results, which can help inexperienced young doctors to make more accurate diagnosis with lesion region information. In this paper, we provide four types of notable baseline architectures in semantic segmentation, which are CNN-based “Encoder-Decoder”, transformer-based “Encoder-Decoder”, U-shape networks and spatial-context based two-branch networks. Specifically, CNN-based “Encoder-Decoder” is a classical segmentation architecture. Transformer-based “Encoder-Decoder” integrates transformers into segmentors to enhance the performance with self-attention mechanism. U-shape networks are widely used on medical image segmentation, such as the widely applied U-Net Ronneberger et al. (2015). Spatial-context based two-branch architecture is another efficient choice. It designs two branches to respectively capture low-level high-resolution features and high-level context features.

Based on baseline segmentors, we then tackle the unsupervised domain adaptation based semantic segmentation task. Recent UDA methods solve the domain shift problem mainly by image alignment Ouyang et al. (2019); Zeng et al. (2021); Chen et al. (2020); Zou et al. (2020) and feature alignment Tsai et al. (2018); Du et al. (2019); Wang et al. (2019); Zeng et al. (2020). In this paper, we propose a feature alignment based method to solve domain shift problem. The motivations can be summarized in the following points: (1) Compared to image alignment based methods, feature alignment based methods always require less computation resource in both training and testing phases. (2) Image alignment based methods show strong power when appearance of source and target images have dramatic difference. Intuitively, the main appearance shift between 2d ultrasound and CEUS images is the color (Fig.1), which means this appearance shift may not cause heavy feature-shift especially on high-level features. (3) Based on the baseline segmentors trained with source images, we directly apply them on target images and find that the segmentation performance on source-trained model does not decrease dramatically compared to the performance on target-trained model. This observation encourages us to explore the potential of feature alignment based method. (4) Image alignment methods mainly utilize “pixel-to-pixel” image translation technique to transform target image into source-style. The inaccuracy and distortion of source-style target image highly harm the segmentation performance. (5) image alignment method depends on generative technique (“pixel-to-pixel” image translation). Compared to feature alignment method, it requires much larger training samples. Obviously, MMOTU image dataset is not that large (OTU_2d and OTU_CEUS respectively contains 1469 and 170 samples), which will lead to unstable optimization and low translation quality. As a whole, feature alignment method is more suitable for the tasks on our proposed dataset.

In this paper, we propose a feature alignment based architecture, which is Dual-Scheme Domain-Selected Network (DS²Net). Specifically, we first design two encoders (E_s and E_t) to map source and target images into two-style features (i.e. E_s will respectively map source and target images into source-style source features and source-style target features. Similar for E_t). Then, we assume that two-style features are not decoupled. It means source-style features may contain some target-style information and vice versa. Based on this assumption, we propose Domain-Distinct-Selected Module (DDSM). With DDSM, we can decouple the source-style (target-style) features into purer source-style (target-style) features and target-style (source-style) features. Obviously, some information may work on both sides or not work on any side. Therefore, we further propose Domain-Universal-Selected-Module (DUSM). With DUSM, we further find the universal information of source/target-style features. Finally, we respectively feed the source-style and target-style features into two decoder-heads (H_s and H_t) for final predictions. During optimization, besides supervision from source annotations, we apply adversarial learning to combat the

domain shift on the two-style features output from E_s and E_t . This design ensures that two-style features can be aligned into same latent space. To prove the effectiveness of DS²Net, we conduct comparison experiments with recent notable feature alignment based domain adaptation methods Tsai et al. (2018); Zeng et al. (2020) on MMOTU image dataset. The experiment results are encouraging.

In summary, the main contributions are listed as follows:

- We construct MMOTU image dataset containing 2d ultrasound and CEUS images. For every images in dataset, we provide pixel-wise semantic annotations and global-wise category annotations.
- To the best of our knowledge, we first propose a method (DS²Net) to tackle the cross-domain ovarian tumor segmentation between 2d ultrasound and CEUS images. With this method, we provide an insight on detecting ovarian tumors on multi-modality ultrasound images.
- DS²Net utilizes domain selected modules (DDSM and DUSM) to extract domain-distinct and domain-universal features. Essentially, we provide an insight on using feature decoupling technique to solve domain shift problem.

2. Related Work

2.1. Computer-Aided Methods on Ovarian Ultrasound Image Datasets

To develop computer-aided methods on medical treatment of ovarian diseases, many methods construct ultrasound image datasets and use DCNNs to tackle the image recognition task. Wu et al. (2018) construct a 2d ultrasound image dataset with three types of ovarian tumors (Benign, Borderline and Malignant). This dataset is used for ovarian tumor classification. Followed Wu et al. (2018), Wang et al. (2021) collect annotated samples of serous ovarian tumors (SOTs) and then apply DCNNs to categorize SOTs into Benign, Borderline and Malignant.

Besides recognition task, many notable methods are proposed to tackle segmentation task on 2d ultrasound ovarian images. These methods mainly aim at characterizing the ovarian structure. Li et al. (2020) propose CR-UNet, which integrates the spatial recurrent neural network (RNN) into a plain U-Net to segment the ovary and follicles. Wanderley et al. (2018) propose fCNN to automatically characterize ovarian structures. Both CR-UNet and fCNN are trained on their collected 2d ultrasound ovarian image datasets with pixel-wise annotations. Recently, several methods have been proposed to characterize the ovarian structure. Mathur et al. (2020) propose S-Net to simultaneously segment ovary and follicles in 3d-ultrasound volumes. Yang et al. (2021) propose C-Rend (contrastive rendering) on ovary and follicles segmentation and further apply it into a semi-supervised learning framework. Both S-Net and C-Rend are trained on their collected 3d-ultrasound ovarian volume datasets.

2.2. Semantic Segmentation on Medical Images

Semantic segmentation has become an widely applied medical image processing technique on many clinical applications, such as organ structure characterization, lesion area detection and cell segmentation. In this field, U-Net Ronneberger et al. (2015) is one of the most famous methods, which creates shortcuts between encoder and decoder to capture contextual and precise localization information. Followed U-Net, U-Net++ Zhou et al. (2018) connects encoder and decoder using a series of nested dense convolutional blocks. Compared to U-Net, this design further bridges the semantic gap between feature maps from encoder to decoder. UcUNet Yang et al. (2023) designs an efficient U-shaped convolution block to increase the network depth with fewer parameters and efficiently ignore invalid features while fusing shallow and deep features. In recent years, attention mechanism substantially promotes semantic segmentation. Oktay et al. (2018) propose an attention U-Net. Before fusing the feature maps from encoder to decoder, attention U-Net inserts an attention gate to control the spatial-wise feature importance. Besides applying spatial-wise attention mechanism, Chen et al. (2019b) propose FED-Net, which uses a channel-wise attention mechanism to improve the performance of liver lesion segmentation. There are also many works Kaul et al. (2019); Paschali et al. (2019); Wang et al. (2020); Zhan et al. (2023) aiming at mixing spatial-wise and channel-wise attention mechanisms.

Transformer is a cutting-edge structure utilizing self-attention mechanism to capture important region of images. On medical image semantic segmentation, TransFuse Zhang et al. (2021) and TransUNet Chen et al. (2021) both employ ViT (Vision Transformer) Dosovitskiy et al. (2021) as encoder for feature extraction. Swin-UNet Cao et al. (2021) applies Swin-Transformer Liu et al. (2021) on both encoder and decoder to explore the learning potential on long-range semantic information. SegTran Li et al. (2021) further proposes a squeeze-and-expansion transformer for more diversified representations. MAXFormer Liang et al. (2023) utilizes an efficient parallel local-global transformer module to enhance accuracy of medical image segmentation for clinical applications.

2.3. Unsupervised Domain Adaptation on Medical Images

UDA mainly aims to alleviate the domain shift problem when applying a source-trained model on target domain data. There are mainly two types of methods on UDA based semantic segmentation task, which are image alignment and feature alignment based methods. Image alignment based methods always adopt image translation Zhu et al. (2017); Isola et al. (2017) to align between source and target images by appearance transformation. Chen et al. (2020) and Ouyang et al. (2019) propose generators for source-to-target transformation and then optimize the segmentor by target-style source images with corresponding annotations. Zou et al. (2020) and Zeng et al. (2021) further add

Table 1

The data distribution of MMOTU image dataset.

Data type	categories	Training set		Testing set	
		samples	patients	samples	patients
OTU_2d	8	1000	171	469	76
OTU_CEUS	8	70	20	100	27

target-to-source generators besides source-to-target generators to bridge source and target domain with a balanced flow. Feature alignment based methods solve the domain shift problem through exploring domain invariant features. Zeng et al. (2020) propose feature and entropy map discriminators to explore the representation potential of domain invariant features. Wang et al. (2019) propose pOSAL to segment the optic disc and optic cup from different fundus image datasets in a joint manner. pOSAL exploits UDA with feature alignment mechanism to ease the domain shift. Dou et al. (2019) propose PnP-AdaNet to tackle domain shift problem by aligning source and target features. On low-level and high-level latent space, it applies adversarial loss for feature-level adaptation. Moreover, some other notable feature alignment based methods, such as AdapSegNet Tsai et al. (2018) and SSF-DAN Du et al. (2019) both achieve great success on both natural scene images and medical images.

There are also many works focusing on disentangling features in unsupervised cross-domain medical image semantic segmentation task. Chen et al. (2019a) and Yang et al. both propose a cross-domain semantic segmentation framework, which decomposes cross-domain images into a domain-invariant content space and domain-specific style space by feature disentanglement module. Both methods achieve outstanding robustness and the generalized capability on cross-domain learning and robust adaptation. Similar to Yang et al.; Chen et al. (2019a), Pei et al. (2021) propose an image alignment based method (DDFSeg) to tackle cross-modality cardiac image segmentation task. Besides extracting domain-invariant features (DIFs), DDFSeg further considers the domain-specific features (DSFs) as complementary features for image translation. With better synthetic source-style target images, the source-trained segmentation network can predict better. To overcome inherent misregistration and disparity in signal intensity on cross-domain images, Chartsias et al. (2021) propose DAFNet to provide improved segmentation accuracy by leveraging information of images of other modalities under unsupervised configuration. DAFNet utilizes disentangled decomposition to disentangle images into semantic anatomy factors and modality factors to map cross-domain images into a smooth latent space. Valindria et al. (2018) and Biase et al. (2021) investigate the feasibility and effectiveness of promoting single-modality medical segmentation with aid of multi-modality information.

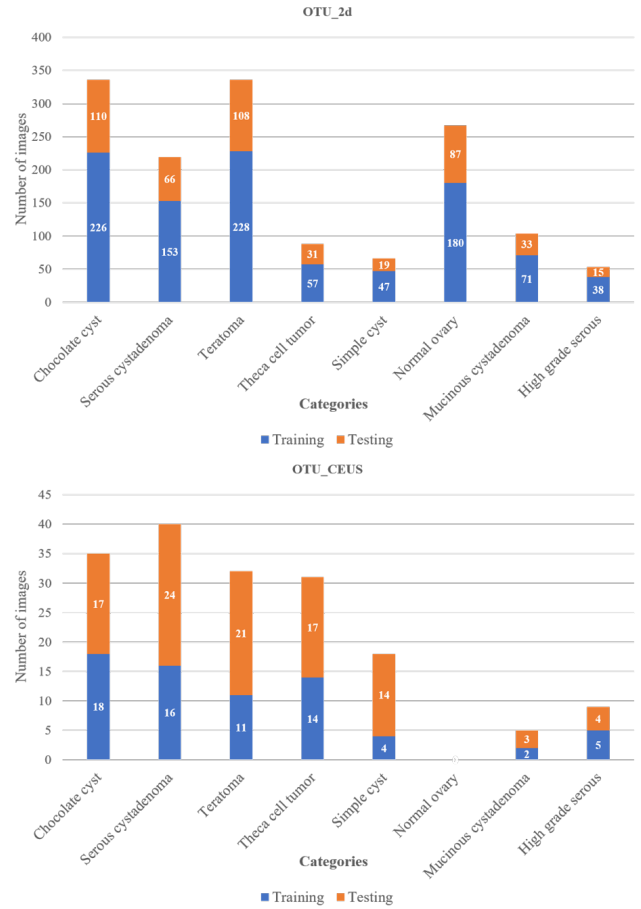


Figure 2: The number of samples containing in each category.

3. Dataset

3.1. Establishment

To tackle the cross-domain ovarian tumor segmentation task, we first propose MMOTU image dataset. All images are obtained from Beijing Shijitan Hospital, Capital Medical University. Our dataset contains 1639 ovarian ultrasound images collected from 294 patients. The scanner is Mindray Resona8 ultrasonic diagnostic instrument. Obviously, each patient is collected with multiple scans. During scanning, doctors select some images (slices), which can clearly show the lesion regions. Sometimes, one slice cannot meet the satisfaction of diagnosis, so doctors will select multiple scans. The main difference between those scans is view. Transvaginal ultrasound scanning is a dynamic process, so multiple scans are extracted from different view angles. As shown in Tab.1, MMOTU image dataset contains two subsets with two modalities, where OTU_2d and OTU_CEUS respectively consist of 1469 2d ultrasound images and 170 CEUS images. On two sub-sets, we split them into training and testing sets. Since each patient is collected with multiple scans, we carefully deal with all samples during splitting dataset to make sure that no “patient-overlapping” between

training and testing sets. The number of patients in training and testing set are shown in Tab.1. It is worth noting that, testing set contains more images than training set in OTU_CEUS, because we hope to guarantee the evaluation quality. When we tackle cross-domain segmentation, more testing images make the results more convincing. Since we will continually collect CEUS images, more samples will be soon added in training set.

MMOTU image dataset has eight typical categories of ovarian tumor (Fig.1). Fig.2 further shows the sample distribution of each category in detail. From Fig.2, we find the following two points. (1) Samples of each category are unbalanced. This is because some types tumors are more common while some types of tumors are rarer in clinical treatment. (2) In OTU_CEUS, some categories only contain few samples, which is easy to cause underfitting. Due to historical and practical reasons, most of the CEUS sequences/images are not stored. Even though we can not provide more samples for those few-shot categories, it is a chance for researchers to conduct researches on few-shot ovarian tumor segmentation or classification. In this research, providing an insight on AI-aided medical treatment using CEUS sequences/images is our main aim. In the future, we will pay attention on preserving and continually collecting CEUS images to extend our OTU_CEUS dataset. (3) “Normal Ovary” category has no sample in OTU_CEUS, because CEUS technology is usually a further examination after 2d ultrasound examination, which is mainly applied to confirm the tumor types (e.g. Benign, Borderline, Malignant or our proposed specific types). It means the CEUS images hardly have “Normal Ovary” category. Under this situation, the segmentation and recognition tasks on OTU_CEUS become seven-category tasks (not eight-category). When tackling UDA segmentation task, no matter OTU_2d is served as source or target set, we will remove the “Normal Ovary” category from OTU_2d to make the experiments reasonable. In other words, UDA segmentation task is also a seven-category task. (4) The segmentation and recognition tasks on OTU_2d are eight-category tasks including “Normal Ovary” category.

For almost every images, only one type of tumor appears. Therefore, we transform an seven/eight-category segmentation task into binary lesion area segmentation task (Task1 and Task2) and tumor recognition task (Task3).

On MMOTU image dataset, the pixel-wise semantic annotations and global-wise category annotations are provided by 27 experts of Obstetrics and Gynecology department. Each image is first annotated by one expert and then checked by another one expert, which guarantees the annotating quality. During annotating, experts refer to pathological reports, which makes the annotations accurate and convincing.

3.2. Data Analysis

In MMOTU image dataset, all images have been analyzed by experts using specialized software, so some symbols like “lines” (Fig.3(a)), “hands” (Fig.3(b)), “characters” (Fig.3(d) and Fig.3(f)) or “arrows” (Fig.3(e)) are marked by them on images. When we collect the images, most

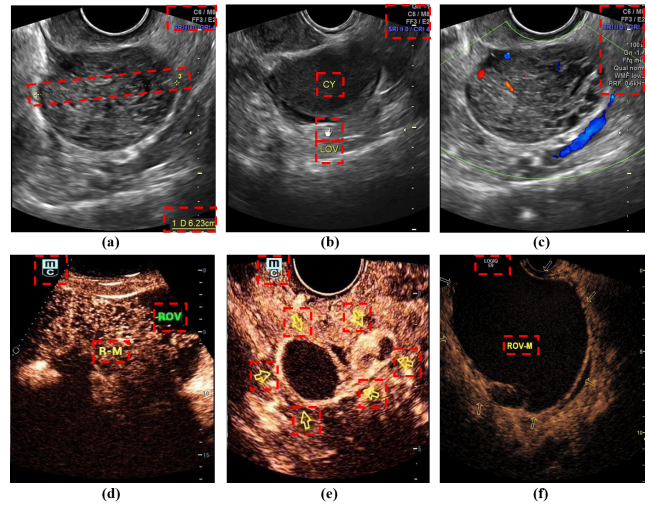


Figure 3: Typical samples in MMOTU image dataset. Images in first and second row are respectively 2d ultrasound and CEUS image samples.

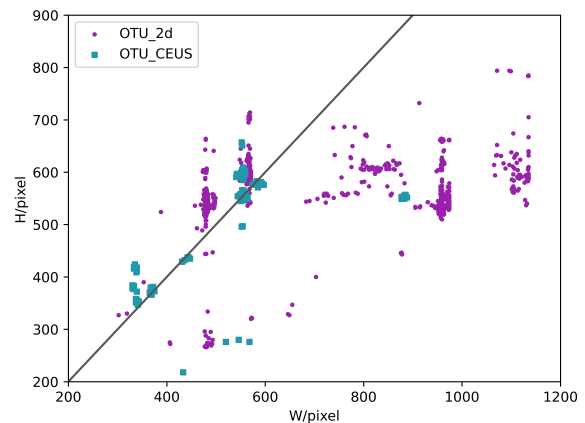


Figure 4: The scatter plot showing the distribution of image scale.

of them contain those symbols. Fig.3 shows some typical samples. Particularly, OTU_2d sub-set contains 216 Color Doppler Flow Images (CDFI), where the rest 1253 images are traditional 2d ultrasound images. Images in OTU_CEUS sub-set are extracted from CEUS sequences. When collecting images, we find that all of them contain private information of patients. According to privacy policy, we manually crop the images to remove the private information and make sure that the published MMOTU image dataset will not contain any private information. For samples from each patient, we provide demographic information including gender, age, weight and doctors’ diagnostic description. To protect patients’ privacy out of ethics, we think that some information (e.g., age, weight) are not supposed be available. However, to maximally help the community investigate and develop the machine learning models based on MMOTU

Table 2

Comparison between MMOTU image dataset and other ovarian ultrasound image dataset. Here, “vol” indicates volumes.

Methods	Data Number	Category Number	Data Type (2d/3d/CEUS)	Task (Cls/Seg/DA-Seg)
Wu et al. (2018)	988	3	✓/✗/✗	✓/✗/✗
Wang et al. (2021)	412	3	✓/✗/✗	✓/✗/✗
Wanderley et al. (2018)	87	3	✓/✗/✗	✗/✓/✗
Li et al. (2020)	3204	3	✓/✗/✗	✗/✓/✗
Narra et al. (2018)	105 (vol)	3	✓/✓/✗	✗/✓/✗
Mathur et al. (2020)	66 (vol)	3	✓/✓/✗	✗/✓/✗
Yang et al. (2021)	307 (vol)	3	✓/✓/✗	✗/✓/✗
Ours	1639	8	✓/✗/✓	✓/✓/✓

image dataset, we’d like to make the doctors’ diagnostic description available after a research request.

As shown in Fig.4, images in dataset have different scales. In OTU_2d, the width and height of images respectively range from 302~1135 and 226~794 pixels. In OTU_CEUS, the width and height of images respectively range from 330~888 and 218~657 pixels. Before training, images are randomly resized and cropped to 384×384 . As mentioned in Sec.1, we hope to measure the tumor size in single-modality segmentation task. Even though the estimation of the physical size of the tumor will be affected when images’ resolutions vary, measurement of tumor size still makes sense when applying MMOTU-trained lesion region segmentation networks on raw images with fixed size.

Tab.2 shows the comparison between MMOTU image dataset and previous ovarian ultrasound image datasets. First, Wu et al. (2018); Wang et al. (2021) construct ovarian 2d ultrasound datasets to train a model which can categorize the ovarian tumor into Benign, Borderline and Malignant. Comparing with their methods, our dataset contains eight concrete ovarian tumor categories (Fig.1). Second, Wanderley et al. (2018); Li et al. (2020); Narra et al. (2018); Mathur et al. (2020); Yang et al. (2021) construct 2d or 3d ultrasound datasets for ovarian structure segmentation. Wanderley et al. (2018); Li et al. (2020) fill their dataset only with 2d ultrasound slices and Narra et al. (2018); Mathur et al. (2020); Yang et al. (2021) fill their dataset with both 2d ultrasound slices and 3d ultrasound volumes. Strictly speaking, 2d ultrasound slices and 3d ultrasound volumes belong to single-modality data, because 2d ultrasound slices are extracted from a specific 3d ultrasound volume. Comparing with their datasets, our dataset contains 2d ultrasound slices together with CEUS images, which is a typical multi-modality dataset. As a whole, we construct MMOTU image dataset to tackle multi-tasks (Fig.1). Moreover, our dataset provides an insight on applying DCNNs for CEUS images.

4. Proposed Method

4.1. Single-Modality Image Segmentation

Based on MMOTU image dataset, we first tackle single-modality semantic segmentation task (Fig.1 Task1) to provide series of baseline segmentors. Fig.5 shows the diagrams

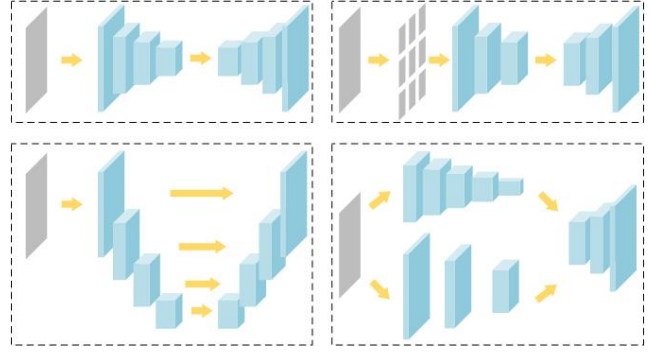


Figure 5: The diagram of recent notable architectures on semantic segmentation. **top-left:** CNN-based “Encoder-Decoder”, **top-right:** Transformer-based “Encoder-Decoder”, **bottom-left:** U-shape networks, **bottom-right:** Spatial-context based two-branch networks.

of four notable architectures in semantic segmentation. For CNN-based “Encoder-Decoder”, we select two notable segmentors, PSPNet Zhao et al. (2017) and DANet Fu et al. (2019). The former utilizes the spatial-wise contextual information, the latter introduces spatial-wise and channel-wise attention information in segmentors. Transformer-based “Encoder-Decoder” is a series of cutting-edge architectures integrating transformers into segmentors to enhance the performance with self-attention mechanism. In this paper, we reimplement SegFormer Xie et al. (2021), which is an efficient and lightweight yet powerful semantic segmentation architecture. U-shape networks are most common-used on medical image segmentation. In this paper, we provide two novel segmentors, which are U-Net Ronneberger et al. (2015). and TransUNet Chen et al. (2021). As another innovative series of segmentors, spatial-context based two-branch networks use “wide-and-shallow” spatial-branch and “narrow-and-deep” context-branch to respectively capture low-level high-resolution and high-level context features. Here, we reimplement BiseNetV2 Yu et al. (2021) as representative of this type of segmentors.

4.2. Unsupervised Domain Adaptation for Semantic Segmentation

Unsupervised domain adaptation (UDA) for semantic segmentation (unsupervised cross-domain semantic segmentation) aims to apply the segmentation network trained from the source domain annotated (labeled) images to the target domain images. It is worth noting that target domain images have no label. Mathematically, given a source domain image dataset $\mathcal{S} = \{(\mathbf{x}^i, \mathbf{y}^i), \forall i = 1, 2, \dots, N\}$ and a target domain image dataset $\mathcal{T} = \{\mathbf{x}^j, \forall j = 1, 2, \dots, M\}$, training set \mathcal{D}_{train} is constructed by \mathcal{S} and \mathcal{T}_{train} (a sub-set of \mathcal{T}). Testing set \mathcal{D}_{test} is constructed by \mathcal{T}_{test} (a sub-set of \mathcal{T}). Then, \mathcal{D}_{train} is used to train a segmentation network, which can predict the images in \mathcal{D}_{test} . Here, $\mathcal{D}_{train} = \mathcal{S} \cup \mathcal{T}_{train}$, $\mathcal{D}_{test} = \mathcal{T}_{test}$, $\mathcal{T} = \mathcal{T}_{train} \cup \mathcal{T}_{test}$, $\mathcal{T}_{train} \cap \mathcal{T}_{test} = \emptyset$, $\mathcal{S} \cap \mathcal{T} = \emptyset$. N and M respectively indicate the sample numbers of source and target domain image datasets. Even

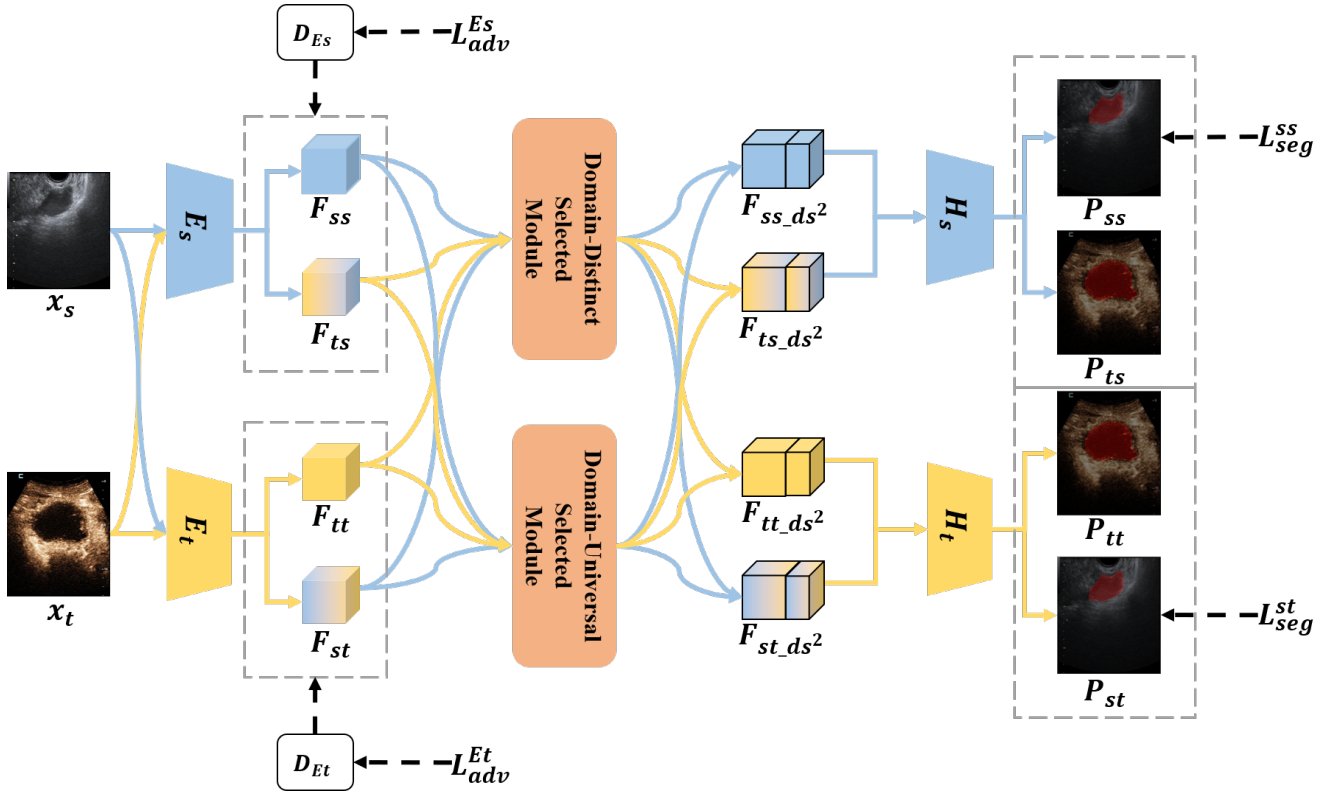


Figure 6: The architecture of DS²Net. Source and target images are first fed into E_s and E_t and the output feature maps are respectively $\{F_{ss}, F_{st}\}$ and $\{F_{tt}, F_{ts}\}$. Then, domain distinct selected module (DDSM) and domain universal selected module (DUSM) are applied on $\{F_{ss}, F_{st}\}$ and $\{F_{tt}, F_{ts}\}$. After processing by DDSM and DUSM, the domain selected features ($\{F_{ss_ds^2}, F_{st_ds^2}\}; \{F_{tt_ds^2}, F_{ts_ds^2}\}$) pass through H_s and H_t to generate final predictions. During optimization, we apply symmetric adversarial loss ($\mathcal{L}_{adv}^{Es}, \mathcal{L}_{adv}^{Et}$) and segmentation loss ($\mathcal{L}_{seg}^{ss}, \mathcal{L}_{seg}^{st}$). Specifically, the discriminators $\{D_{Es}, D_{Et}\}$ are designed for feature alignment. During inference, we apply ensemble strategy to integrate the two predictions of target images ($\{P_{tt}, P_{ts}\}$).

though target images appear in training process, no label is provided. Therefore, this training process can be regarded as “unsupervised”.

In this paper, exploiting the potential of lesion area segmentation for bidirectional UDA between 2d ultrasound and CEUS images is our main focus. When OTU_2d is served as source domain image dataset, OTU_CEUS will be served as target domain image dataset and vice versa. To solve the domain shift problem, we propose a feature alignment based method, DS²Net. The overview of the architecture is shown in Fig.6. DS²Net utilizes adversarial learning to alleviate the representation gap between source and target domain images. Based on feature alignment, DS²Net disentangles and fuses 2d ultrasound and CEUS features to tackle multi-modality segmentation task. Essentially, adversarial learning first maps source and target features into same latent space. Then, DDSM and DUSM respectively find domain distinct and universal representations.

4.2.1. Adversarial Learning for Feature Alignment

As shown in Fig.6, we respectively design E_s and E_t for feature extraction of source and target images. Obviously, we expect that both E_s and E_t have the general representation

capability on source and target images. Therefore, we apply adversarial learning on E_s and E_t to alleviate the representation gap caused by domain shift. This process is formulated from Eq.1 to Eq.4.

$$\mathcal{L}_{adv}^{Es}(E_s, D_{Es}) = \mathbb{E}_{x_s \sim X^s}[\log(D_{Es}(F_{ss}))] + \mathbb{E}_{x_t \sim X^t}[\log(1 - D_{Es}(F_{ts}))] \quad (1)$$

$$F_{ss} = E_s(x_s), \quad F_{ts} = E_s(x_t) \quad (2)$$

$$\mathcal{L}_{adv}^{Et}(E_t, D_{Et}) = \mathbb{E}_{x_t \sim X^t}[\log(D_{Et}(F_{tt}))] + \mathbb{E}_{x_s \sim X^s}[\log(1 - D_{Et}(F_{st}))] \quad (3)$$

$$F_{tt} = E_t(x_t), \quad F_{st} = E_t(x_s) \quad (4)$$

Here, x_s and x_t respectively denote source and target images. D_{Es} and D_{Et} are two discriminators. $F_{ss}, F_{ts}, F_{tt}, F_{st}$ are respectively denoted as source-style source feature, source-style target feature, target-style target feature and target-style source feature. We adopt min-max criterion to

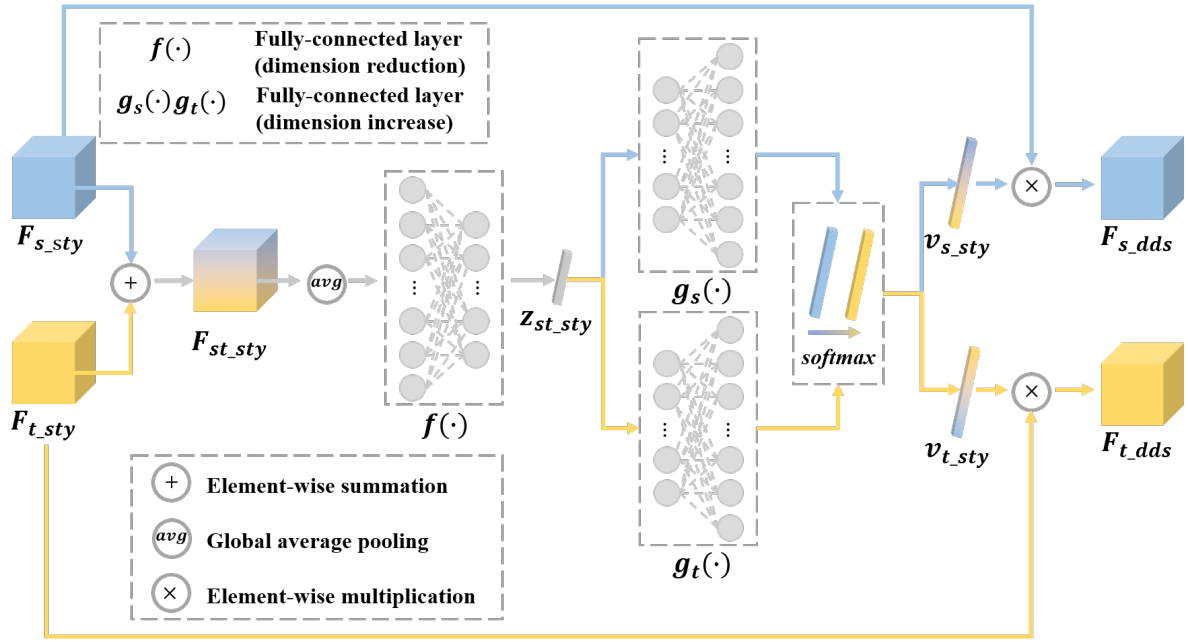


Figure 7: The architecture of domain-distinct selected module. Here, $\{F_{s_sty}, F_{t_sty}\}$ are respectively source-style and target-style features of source or target images ($\{F_{ss}, F_{st}\}$ or $\{F_{tt}, F_{ts}\}$). Two-style features are first integrated to generate a fused prototype (z_{st_sty}). Then, we adopt channel-wise attention to obtain channel-wise weighted vectors ($\{v_{s_sty}, v_{t_sty}\}$) for F_{s_sty} and F_{t_sty} . Finally, we multiply $\{v_{s_sty}, v_{t_sty}\}$ on F_{s_sty} and F_{t_sty} in channel-wise to obtain domain distinct features ($\{F_{s_dds}, F_{t_dds}\}$).

optimize E_s and E_t , formulated as $\min_{E_s} \max_{D_{E_s}} \mathcal{L}_{adv}^{E_s}(E_s, D_{E_s})$ and $\min_{E_t} \max_{D_{E_t}} \mathcal{L}_{adv}^{E_t}(E_t, D_{E_t})$. With this feature alignment on E_s and E_t , two encoders have better ability to represent images from two domains. Furthermore, two encoders can provide one more feature map for image from each domain, which enriches the representations.

4.2.2. Domain Distinct & Domain Universal Selected Modules

As shown in Eq.2 and Eq.4, we design two encoders to extract source-style and target-style features for source and target images. Based on the observation that directly applying a source-trained segmentation model on target images will not cause dramatic performance decrease, we make the following assumptions. (1) Between 2d ultrasound and CEUS images, there may exist some easy-extracted universal features, which have positive influence on segmenting images from both two domains. (2) Since there still exists some performance gap when simply evaluating target images on source-trained models, we believe that domain distinct features also exist. (3) Distinct and universal features can be decoupled from source-style and target-style features. Instructed by the above assumptions, we design Domain Distinct Selected Modules (DDSM) and Domain Universal Selected Modules (DUSM).

DDSM: As shown in Fig.6, source and target images are both represented as source-style and target-style features, which respectively are $\{F_{ss}, F_{st}\}$ ($\mathbb{R}^{C \times H \times W}$) and $\{F_{tt}, F_{ts}\}$ ($\mathbb{R}^{C \times H \times W}$). After applying adversarial learning, E_s and E_t can better represent two domain images as source-style

and target-style features. To further extract purer feature specifically for each domain, we propose DDSM.

As shown in Fig.7 and Eq.5, we first fuse source-style and target-style features. Then, we apply global average pooling and a dimension-reduction fully-connected layer ($f(\cdot)$) to generate a global-wise fused prototype ($z_{st_sty} \in \mathbb{R}^{C \times 1 \times 1}$).

$$\begin{aligned} z_{st_sty} &= f\left(\frac{1}{HW} \sum_{h=1}^H \sum_{w=1}^W (F_{st_sty}(h, w))\right) \\ &= f\left(\frac{1}{HW} \sum_{h=1}^H \sum_{w=1}^W (F_{s_sty}(h, w) + F_{t_sty}(h, w))\right) \end{aligned} \quad (5)$$

Then, we serve z_{st_sty} as guidance to create channel-wise weighted vectors (v_{s_sty} and $v_{t_sty} \in \mathbb{R}^{C \times 1 \times 1}$) using *softmax* operation shown in Eq.6 and Eq.7. $g_s(\cdot)$ and $g_t(\cdot)$ are dimension-increase fully-connected layers.

$$v_{s_sty} = \frac{e^{g_s(z_{st_sty})}}{e^{g_s(z_{st_sty})} + e^{g_t(z_{st_sty})}} \quad (6)$$

$$v_{t_sty} = \frac{e^{g_t(z_{st_sty})}}{e^{g_s(z_{st_sty})} + e^{g_t(z_{st_sty})}} \quad (7)$$

Finally, the domain distinct selected features (F_{s_dds} and $F_{t_dds} \in \mathbb{R}^{C \times H \times W}$) are calculated through channel-wise multiplication shown in Eq.8.

$$F_{s_dds} = F_{s_sty} \times v_{s_sty}, \quad F_{t_dds} = F_{t_sty} \times v_{t_sty} \quad (8)$$

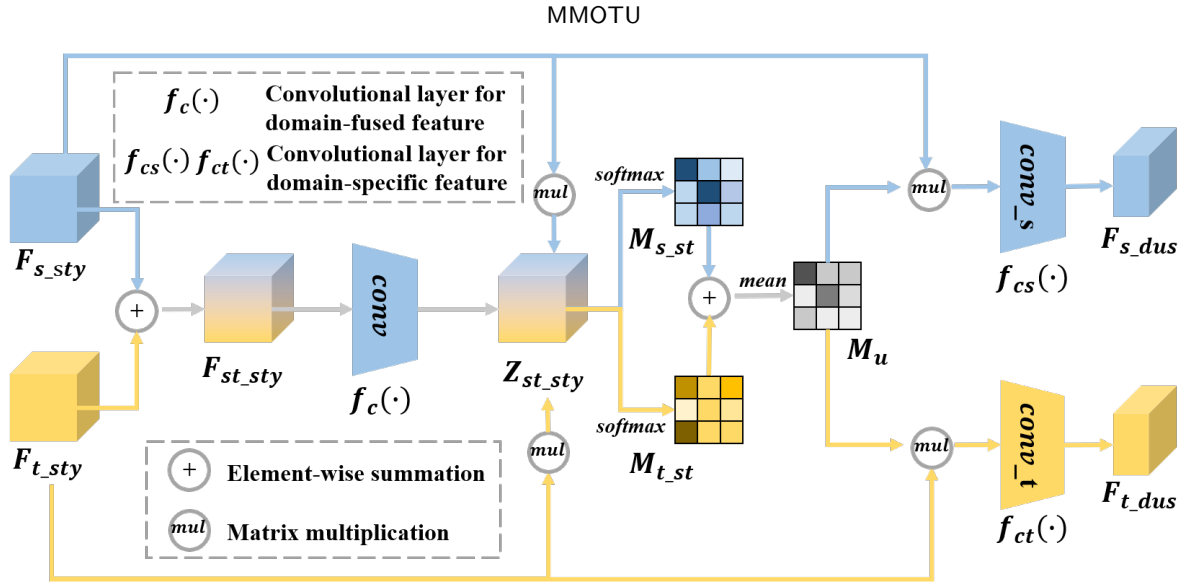


Figure 8: The architecture of domain-universal selected module. Two-style features are first integrated to generate a fused feature (Z_{st_sty}). Then, we adopt matrix multiplication operation to obtain attention masks ($\{M_{s_sty}, M_{t_sty}\}$) for F_{s_sty} and F_{t_sty} . Next, we average M_{s_sty} and M_{t_sty} for a universal attention mask (M_u). Finally, we serve M_u as universal guidance on F_{s_sty} and F_{t_sty} to obtain domain universal features ($\{F_{s_dus}, F_{t_dus}\}$).

From Eq.6 to Eq.7, we find that $v_{s_sty} + v_{t_sty} = \mathbf{1}$, which means we force the source-style and target-style features to have complementary channel combinations. With this design, “source-style features are more source-style while target-style features are more target-style”.

DUSM: With DDSM, we obtain purer source-style and target-style features, but it may overlook the universal features benefiting both source and target images. Therefore, we further design DUSM to extract universal features of F_{s_sty} and F_{t_sty} . As shown in Fig.8, we first fuse source-style and target-style features similar to DDSM (Eq.9).

$$\begin{aligned} Z_{st_sty} &= f_c\left(\frac{1}{HW} \sum_{h=1}^H \sum_{w=1}^W (F_{st_sty}(h, w))\right) \\ &= f_c\left(\frac{1}{HW} \sum_{h=1}^H \sum_{w=1}^W (F_{s_sty}(h, w) + F_{t_sty}(h, w))\right) \end{aligned} \quad (9)$$

Here, Z_{st_sty} ($\mathbb{R}^{C \times H \times W}$) represent domain fused feature. We then perform matrix multiplication between Z_{st_sty} and $\{F_{s_sty}, F_{t_sty}\}$. The output attention masks ($\{M_{s_st}, M_{t_st}\} \in \mathbb{R}^{C \times C}$) are averaged for universal attention mask ($M_u \in \mathbb{R}^{C \times C}$). This process is shown in Eq.10 ~ Eq.12.

$$M_{s_st}(j, i) = \frac{e^{F_{s_sty}(i) \cdot Z_{st_sty}(j)}}}{\sum_{i=1}^C (e^{F_{s_sty}(i) \cdot Z_{st_sty}(j)})} \quad (10)$$

$$M_{t_st}(j, i) = \frac{e^{F_{t_sty}(i) \cdot Z_{st_sty}(j)}}}{\sum_{i=1}^C (e^{F_{t_sty}(i) \cdot Z_{st_sty}(j)})} \quad (11)$$

$$M_u(j, i) = \frac{M_{s_st}(j, i) + M_{t_st}(j, i)}{2} \quad (12)$$

where F_{s_sty} , F_{t_sty} and Z_{st_sty} are reshaped to $\mathbb{R}^{C \times (HW)}$. “ (j, i) ” indicates the impact measurement between i^{th} channel of $\{F_{s_sty}, F_{t_sty}\}$ and j^{th} channel of Z_{st_sty} .

Finally, we use M_u to extract the universal feature from F_{s_sty} and F_{t_sty} , which are F_{s_dus} and F_{t_dus} ($\mathbb{R}^{C'' \times H \times W}$). This formulation is shown in Eq.13.

$$F_{s_dus} = f_{cs}(M_u * F_{s_sty}), \quad F_{t_dus} = f_{ct}(M_u * F_{t_sty}) \quad (13)$$

In summary, we extract the universal feature by finding M_u , which measures the joint impact between source/target-style features and domain fused feature. The larger element in M_u indicates that one channel of fused domain features has high impact both on same channel of source-style and target-style features. Essentially, we utilize a domain universal attention mask to select the universal features in channel-wise manner.

Analysis between DDSM and DUSM: Generally, two modules both focus on improving the feature-level understanding for target domain images. The main differences between DDSM and DUSM can be listed in the following aspects. (1) Motivation differences. Motivated by decoupling and extracting domain-distinct features, we design DDSM. Motivated by selecting and extracting domain-universal features, we design DUSM. (2) Designing principle differences. As shown in Fig.7, DDSM decouples fused features (F_{st_sty}) by extracting opposing and complementary channel-wise attention (channel-wise weighted vectors) for two-style features. As shown in Fig.8, DDUM extracts universal features by finding the channel-wise universal attention mask (M_u). (3) Feature extraction differences. DDSM utilizes global-level features to decouple distinct features while DUSM utilizes semantic-level features to finding universal features.

4.2.3. Optimization

In this paper, we apply segmentation loss and adversarial loss to jointly optimize the DS²Net. As for segmentation loss, We apply cross-entropy loss, formulated in Eq.14.

$$\begin{aligned} \mathcal{L}_{seg}(E_s, H_s, E_t, H_t) &= \mathcal{L}_{seg}^{ss}(E_s, H_s) + \mathcal{L}_{seg}^{st}(E_t, H_t) \\ &= \mathbb{E}_{x^s \sim \mathcal{X}^s}[-y_s \log(H_s(F_{ss_ds^2}))] \\ &\quad + \mathbb{E}_{x^s \sim \mathcal{X}^s}[-y_s \log(H_t(F_{st_ds^2}))] \end{aligned} \quad (14)$$

where H_s and H_t are two decoder-heads respectively designed for source-style and target-style features. $F_{ss_ds^2} = \text{cat}(F_{ss_dds}, F_{ss_dus})$; $F_{st_ds^2} = \text{cat}(F_{st_dds}, F_{st_dus})$. “cat” denotes concatenation. As shown in Eq.8, Eq.13, $\{F_{ss_ds^2}, F_{st_ds^2}\} \in \mathbb{R}^{(C+C') \times H \times W}$.

To optimize the whole architecture, we apply combined loss (\mathcal{L}) shown in Eq.15. $\{\lambda_{adv}^{E_t}, \lambda_{adv}^{E_s}\}$ are trade-off hyper-parameters adjusting the impact of each loss item.

$$\begin{aligned} \mathcal{L} &= \mathcal{L}_{seg}(E_s, H_s, E_t, H_t) \\ &\quad + \lambda_{adv}^{E_s} \mathcal{L}_{adv}^{E_s}(E_s, D_{E_s}) + \lambda_{adv}^{E_t} \mathcal{L}_{adv}^{E_t}(E_t, D_{E_t}) \end{aligned} \quad (15)$$

From the perspective of backward optimization process, we find the following points. (1) Through adversarial learning, E_s and E_t have the basic representation ability on source and target images avoiding representation distortion of target images. (2) Based on adversarial learning and DDSM/DUSM, the segmentation loss ($\mathcal{L}_{seg}^{ss}(E_s, H_s)$ and $\mathcal{L}_{seg}^{st}(E_t, H_t)$) can force $\{E_s, H_s\}$ and $\{E_t, H_t\}$ to have specific representation trend (e.g. $\{E_t, H_t\}$ tends to represent source and target images into target style). Optimized like this, the architecture becomes more friendly to target images.

4.2.4. Inference

As shown in Eq.2 and Eq.4, target image (x_t) first passes through E_s and E_t to generate F_{ts} and F_{tt} . Then F_{ts} and F_{tt} are respectively fed into DDSM and DUSM to generate domain distinct features ($\{F_{ts_dds}, F_{tt_dds}\}$) and domain universal features ($\{F_{ts_dus}, F_{tt_dus}\}$). Next, different style features are concatenated together, which can be expressed as $F_{ts_ds^2} = \text{cat}(F_{ts_dds}, F_{ts_dus})$ and $F_{tt_ds^2} = \text{cat}(F_{tt_dds}, F_{tt_dus})$. Finally, we use two decoder-heads to map these features into two predictions ($\{P_{ts}, P_{tt}\}$) and integrate them for final prediction (P_t), shown in Eq.16.

$$P_t = \frac{P_{ts} + P_{tt}}{2} = \frac{H_s(F_{ts_ds^2}) + H_t(F_{tt_ds^2})}{2} \quad (16)$$

Here, P_{ts} and P_{tt} are *softmax* predictions (posterior probabilities). Inspired by ensemble learning, we apply soft voting to integrate two predictions. The predictive segmentation mask can be calculated by $\arg \max(\cdot)$ operation.

5. Experiments and Analysis

5.1. Single-Modality Semantic Segmentation

5.1.1. Implementation Details

As mentioned in Sec.4 and Fig.5, we reimplement the six baseline segmentors on MMOTU image dataset. Before

Table 3

Implementation details of single-modality semantic segmentation. “†” means loading ImageNet-pretrained weights Deng et al. (2009). “Res50”, “mit_b5” “ViT” respectively denote ResNet-50 He et al. (2016), Mix Transformer Xie et al. (2021) and Vision Transformer Dosovitskiy et al. (2021).

Methods	Optimizer	Initial LR	LR Decay	Backbone	Iterations
PSPNet	SGD	0.01	poly	Res50 [†]	80k
DANet	SGD	0.01	poly	Res50 [†]	80k
SegFormer	Adam	0.00006	poly	mit_b5 [†]	80k
U-Net	SGD	0.01	poly	U-Net [†]	80k
TransUNet	SGD	0.01	poly	Res50+ViT [†]	80k
BiseNetV2	SGD	0.05	poly	BiseNetV2 [†]	80k

training, input images are randomly resized and cropped to 384×384 . A series of data augmentation methods, such as “RandomFlip” are applied. Towards the four types of segmentors, the implementation details are shown in Tab.3. Here, when optimizer is SGD, the momentum is set as 0.9 and the weight decay value is 0.0005. When optimizer is Adam, the weight decay value is 0.01. All segmentors adopt “poly” to adjust learning rate and the power is set to 0.9.

As shown in Tab.3, SegFormer is optimized with Adam while other segmentation networks are optimized with SGD. Moreover, different networks use different learning rates. To reimplement baseline segmentors on single-modality semantic segmentation task for our proposed MMOTU image dataset, we mainly follow these methods’ original training implementation details, which leads to different configurations in Tab.3. Technically, we select six baseline segmentation networks according to four types of architectures (Fig.5). Among the six networks, SegFormer belongs to Transformer-based network while PSPNet, DANet, U-Net and BiseNetV2 belong to CNN-based networks. Transformer and CNN have large structural discrepancy, so we select suitable optimizer and learning rate based on previous knowledge and experimental experience to ensure that each network can boost its performance. In addition, TransUNet is a CNN-Transformer integrated network. Since large number of trainable parameters are from CNN, we select same configuration as CNN-based networks.

5.1.2. Experimental Results

The single-modality segmentation results are shown in Tab.4. The *IoU* value indicates the intersection of union between predicted and annotated lesion area. The *mIoU* value indicates the average *IoU* value of lesion area and background. Tab.4 shows that U-Net and BiseNetV2 perform poorer compared to other methods. DANet and SegFormer respectively outperform other methods on OTU_2d and OTU_CEUS. Particularly on OTU_CEUS, with less training samples, SegFormer shows much stronger performance. From Tab.4, we can find that PSPNet and SegFormer

Table 4

Single-modality segmentation results on MMOTU image dataset. We adopt *IoU* (Intersection over Union) as metric.

Methods	OTU_2d		OTU_CEUS	
	<i>IoU</i> (%)	<i>mIoU</i> (%)	<i>IoU</i> (%)	<i>mIoU</i> (%)
PSPNet	82.24	89.66	71.35	81.64
DANet	82.58	89.97	70.69	81.87
SegFormer	82.46	89.88	73.03	83.00
U-Net	79.91	86.80	69.18	80.04
TransUNet	81.31	89.01	70.15	80.82
BiseNetV2	79.37	86.13	70.25	80.98

Table 5

Training details of cross-domain semantic segmentation. DS²Net_P and DS²Net_T respectively denote the DS²Net following PSPNet and SegFormer.

Methods	Encoders/DDSM/DUSM		Decoder-Heads		Discriminator	
	optimizer	initial (LR)	optimizer	initial (LR)	optimizer	initial (LR)
DS ² Net_P	SGD	0.01	SGD	0.02	Adam	0.00025
DS ² Net_T	Adam	0.00006	Adam	0.00001	Adam	0.00001

perform more balanced on two sub-sets. Therefore, we select them as baseline segmentors to construct DS²Net for the following cross-domain semantic segmentation task.

5.2. Cross-Domain Semantic Segmentation

5.2.1. Implementation Details

As shown in Fig.6, DS²Net is a symmetric ‘‘Encoder-Decoder’’ architecture. Since PSPNet and SegFormer are notable ‘‘Encoder-Decoder’’, we follow them to design DS²Net. Specifically, DS²Net_P and DS²Net_T respectively inherit the encoder and decoder of PSPNet and SegFormer. DS²Net_P adopts ResNet-50 as encoders (E_s, E_t) and ‘‘PSPHead’’ as decoder-heads (H_s, H_t). DS²Net_T adopts ‘‘Hierarchical Transformer’’ as encoders and ‘‘All-MLP’’ as decoder-heads. As shown in Tab.5, DS²Net_P and DS²Net_T use different implementation configurations mainly because of the large structural discrepancy between Transformer and CNN. For two discriminators ($\{D_{E_s}, D_{E_t}\}$), we follow the common-applied configuration of PatchGAN Isola et al. (2017). $\{D_{E_s}, D_{E_t}\}$ consist of 4 convolutional layers with kernels as size of 4×4 . The stride of the first two layers is 2 while the the last two layers set the stride as 1. The output channels of each layer are {64, 128, 256, 1}. The training details are shown in Tab.5. Additionally, we select binary cross entropy loss as adversarial loss function and the training factors ($\{\lambda_{adv}^{E_t}, \lambda_{adv}^{E_t}\}$) are set as 0.005.

5.2.2. No Domain Adaptation Experiments

Before evaluating the domain adaptation performance of DS²Net on MMOTU image dataset, we first conduct no domain adaptation experiment. In this experiment, PSPNet

Table 6

Comparison between single-modality segmentation and no domain adaptation (w/o DA) segmentation. The left and right of \rightarrow indicate source and target dataset respectively. Results of PSPNet and SegFormer are obtained by training and evaluating on single-modality target dataset.

Methods	OTU_CEUS \rightarrow OTU_2d		OTU_2d \rightarrow OTU_CEUS	
	<i>IoU</i> (%)	<i>mIoU</i> (%)	<i>IoU</i> (%)	<i>mIoU</i> (%)
PSPNet	82.24	89.66	71.35	81.64
PSPNet (w/o DA)	44.17	66.95	50.22	67.60
SegFormer	82.46	89.88	73.03	83.00
SegFormer (w/o DA)	56.28	74.04	61.11	75.45

Table 7

5-Fold cross-validation tests on UDA cross-modality ovarian lesion area semantic segmentation. Results are reported as ‘‘mean \pm standard deviation’’.

Methods	OTU_CEUS \rightarrow OTU_2d		OTU_2d \rightarrow OTU_CEUS	
	<i>IoU</i> (%)	<i>mIoU</i> (%)	<i>IoU</i> (%)	<i>mIoU</i> (%)
AdapSegNet_P	47.50 \pm 2.73	66.15 \pm 2.51	55.08 \pm 2.12	70.24 \pm 1.83
EGUDA_P	48.91 \pm 1.85	67.94 \pm 1.89	56.76 \pm 1.59	72.19 \pm 1.40
DS ² Net_P (ours)	52.73 \pm 1.51	71.87 \pm 1.35	60.21 \pm 1.26	74.38 \pm 1.01
AdapSegNet_T	62.37 \pm 3.29	76.06 \pm 2.46	63.17 \pm 2.27	76.17 \pm 2.11
EGUDA_T	58.06 \pm 2.62	73.12 \pm 1.99	59.72 \pm 1.96	74.78 \pm 2.80
DDFseg	55.92 \pm 5.38	72.85 \pm 4.39	60.94 \pm 4.13	74.59 \pm 3.53
DAFormer	62.76 \pm 2.78	76.52 \pm 2.14	58.52 \pm 2.41	73.97 \pm 2.61
DCLA	61.53 \pm 4.79	75.31 \pm 4.67	60.20 \pm 5.16	74.88 \pm 4.74
EDRL	63.05 \pm 6.13	76.63 \pm 5.45	57.41 \pm 4.86	72.95 \pm 4.07
DS ² Net_T (ours)	64.67\pm2.34	78.12\pm1.97	68.73\pm1.67	79.59\pm1.50

and SegFormer are trained by source annotated samples and evaluated on target samples using the configurations in Tab.3. The results are shown in Tab.6. Previous methods Chen et al. (2020); Zou et al. (2020) apply no domain adaptation experiment between CT and MR images. The segmentation results always dramatically decrease (40~60% lower than single-modality training). Compared to previous results, our results on domain adaptation do not decrease by large margin, E.g., when SegFormer is trained with OTU_2d and evaluated on OTU_CEUS, the *IoU* value decreases by 11.92% (73.03% \sim 61.11%) comparing with target-trained SegFormer. It worth noting that the results training with OTU_2d and evaluating on OTU_CEUS are more valuable, because OTU_2d has more training samples than OTU_CEUS (Tab.1). No domain adaptation experiments results inspire us to explore the potential of feature alignment and distinct/universal feature extraction.

5.2.3. Cross-Domain Semantic Segmentation Experiments

To prove the effectiveness of DS²Net, we re implement two notable feature-alignment based methods, which are AdapSegNet Tsai et al. (2018) and EGUDA Zeng et al. (2020) on MMOTU image dataset. For fairly comparison, minor modifications are applied. For AdapSegNet

Table 8

Ablation experiments adapting OTU_2d to OTU_CEUS. “Symmetric” denotes the symmetric architecture with dual encoders and decoder-heads, i.e. DS²Net removing D_{E_s} , D_{E_t} , DDSM and DUSM (Fig.6). “+” means appending.

Methods	\mathcal{L}_{seg}^{ss}	\mathcal{L}_{seg}^{st}	$\mathcal{L}_{adv}^{E_s}$	$\mathcal{L}_{adv}^{E_t}$	IoU(%)	mIoU(%)
PSPNet (w/o DA)	-	-	-	-	50.22	67.60
+ Symmetric (w/o DA)	✓	✓	-	-	50.54	67.81
+ Feature alignment (FA)	✓	✓	✓	✓	57.08	72.55
+ DDSM	✓	✓	✓	✓	59.28	74.53
+ DUSM (DS ² Net_P)	✓	✓	✓	✓	61.85	75.75
SegFormer (w/o DA)	-	-	-	-	61.11	75.45
+ Symmetric (w/o DA)	✓	✓	-	-	61.01	75.33
+ Feature alignment (FA)	✓	✓	✓	✓	64.74	77.54
+ DDSM	✓	✓	✓	✓	68.06	79.78
+ DUSM (DS ² Net_T)	✓	✓	✓	✓	69.81	80.86

and EGUDA, we respectively replace the original shared segmentation network and segmentor with PSPNet or SegFormer. For the discriminator, we adopt the same PatchGAN as $\{D_{E_s}, D_{E_t}\}$ of DS²Net. We further reimplement 4 recent notable methods (DDFSeg Pei et al. (2021), DAFormer Hoyer et al. (2022), EDRL Wang et al. (2023) and DCLA Li et al. (2023)) following their original model configurations. Specifically, DDFSSeg, EDRL and DCLA are typical image alignment methods with feature disentanglement mechanism. DAFormer is a novel self-training based method. In addition, these 4 methods are not feature-alignment methods with typical “Encoder-Decoder” architecture.

To rigorously compare DS²Net with previous methods, we conduct 5-Fold cross-validation tests on cross-domain semantic segmentation task. Specifically, we randomly split original training set into 5 parts, where 4 parts are used for training while the rest one is used for validation. The best model on validation set is used for testing. Under this configuration, there may have overlapping samples (different scans from same patients) between training and validation sets. Strictly speaking, training and validation sets are supposed to be independent. Since the aim of cross-validation is to select the best-performed model on testing set, it is still reliable to select best-performed model on validation set with small number of random overlapping samples in training set.

Tab.7 shows the comparison results. Generally, our proposed DS²Net performs much stronger than previous methods. Specifically, From experimental results shown in Tab.7, we analyze in the following points. (1) In recent year, Transformer structure has been proved that it can outperform CNN structure in various vision tasks. However, it is more unstable in training phrase. The results in Tab.7 show that SegFormer and DS²Net_T respectively has less bias but larger variance than PSPNet and DS²Net_P. (2) When DS²Net is trained on OTU_CEUS and evaluated on OTU_2d, DS²Net has larger variance compared to model trained on OTU_2d and evaluated on OTU_CEUS. The reason is that OTU_CEUS has far smaller number of training samples than OTU_2d, which leads to larger performance

fluctuation. (3) DDFSSeg and EDRL apply feature disentanglement mainly for better image translation. DCLA designs domain translation path, which also a typical image alignment methods. On MMOTU image dataset with small domain shift and small training set, three methods suffer from large performance fluctuation. DAFormer achieves competitive results, which benefits from Transformer encoder and self-training strategy. However, on binary segmentation task, it is easy to overfit on foreground category. (4) AdapSegNet, EGUDA, DDFSSeg, DAFormer, EDRL and DCLA are all generalized and notable methods on UDA medical semantic segmentation task. Compared to them, DS²Net is more suitable for specific data distribution and UDA task configuration of our proposed MMOTU image dataset, DS²Net performs best among these four methods.

5.2.4. Ablation Study

To separately prove the efficiency of each module of DS²Net, we conduct experiments adapting OTU_2d to OTU_CEUS. From Tab. 8, we analyze in the following points. (1) Compared to PSPNet without domain adaptation, only applying symmetric structure can not bring improvement, because domain shift problem still exists. (2) When adding feature alignment mechanism, the performance significantly improve. This reflects that feature alignment makes effect on alleviating the domain shift problem and improves the general representation capability of E_s and E_t . (3) When appending DDSM, the architecture further improves. The reason is that DDSM guides the optimization trend making the target images become easier to be represented into target-style. (4) When appending DUSM, the architecture still achieves improvement benefiting from universal feature extraction. (5) As shown in Tab.8, DDSM and DUSM can work well singly. When applying two modules together, the cross-domain semantic segmentation performance further improves. It means two modules are compatible and have complementary contributions on performance improvement. (6) In this experiment, DS²Net is trained on training set and directly evaluated on testing set at each 4k iterations (80k iterations in total). We find a best performance model on testing set and provide the best results to reveal the effectiveness of each key module.

5.2.5. Visualization and Analysis

To intuitively show the performance of DS²Net, we compare the segmentation performance of different methods. The qualitative results are shown in Fig.9. We can observe that training model under “w/o DA” setting can work well on some easy cases, but cannot handle harder cases. Benefiting from feature alignment mechanism, AdapSegNet and EGUDA can generate reasonable predictions under most cases, even on hard cases. DDFSSeg and DAFormer can also perform well, in which DAFormer has more tendency on foreground prediction because of pseudo-foreground-label guidance (self-training mechanism). Obviously, DS²Net shows the most powerful performance compared to previous methods. On medium and hard cases, our proposed DS²Net

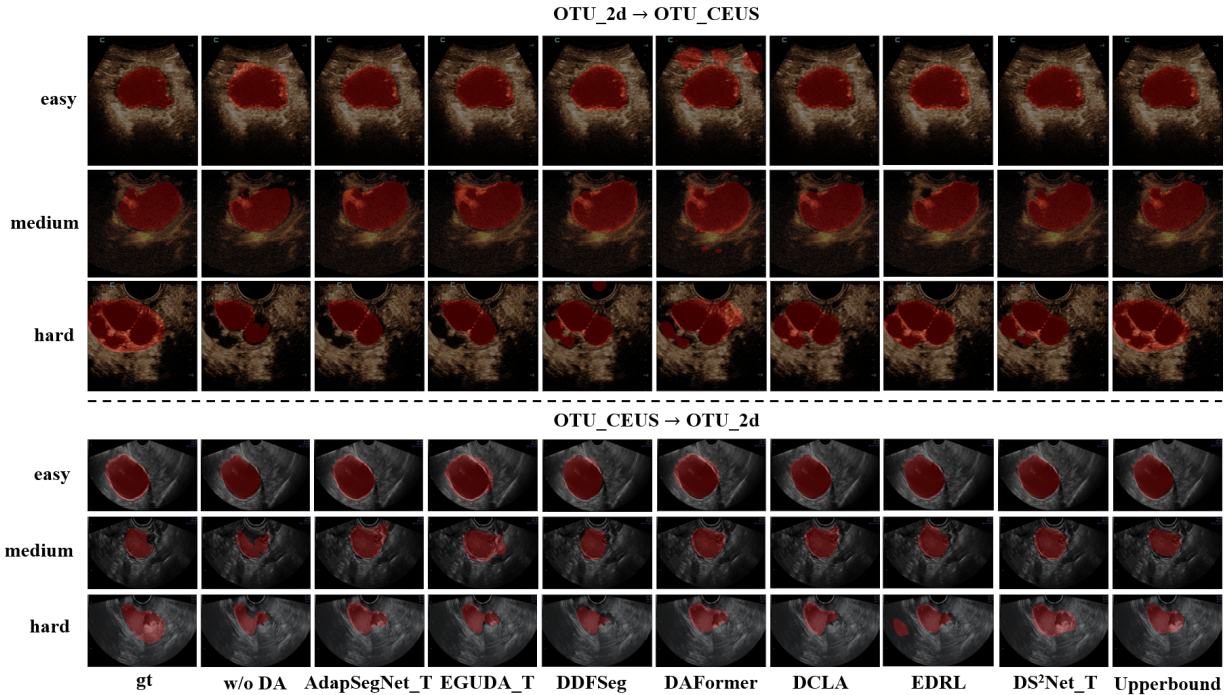


Figure 9: Visualization comparison between different methods. We select SegFormer-based models as example. “Upperbound” indicates the results from single-modality training model.

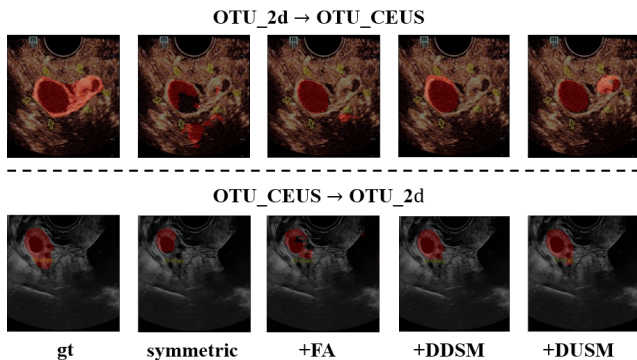


Figure 10: Visualization comparison to illustrate the effectiveness of each module. We select segformer-based models as example.

can capture more semantic information and achieve closest results to “Upperbound”.

To directly show the effectiveness of each module, we also conduct visualization analysis. As shown in Fig.10, symmetric architecture does not work well, because dual encoders and decoder-heads can not solve domain shift problem. When applying feature alignment mechanism, the model can generate reasonable predictions. When appending DDSM, the model shows stronger generalization power on target images. Intuitively, models with DDSM decrease obvious false positive predictive regions and avoid obvious missing detection. When adding DUSM, the final DS²Net

shows the strongest representation capability with better semantic understanding on target images, which can localize more “hard-finding” lesion regions. This visualization comparison coincides with the ablation experiments shown in Tab.8, which further proves the interpretability of DS²Net in an intuitive manner.

5.2.6. Generalization Analysis

To demonstrate the generalization of our proposed DS²Net, we further conduct experiments on MM-WHS (Multi-Modality Whole Heart Segmentation) Zhuang and Shen (2016); Wu and Zhuang (2020), which is a notable cross-modality medical image dataset including CT and MR images¹. This dataset consists of 52 CT images and 46 MR images, where 20 CT and 20 MR are labeled with gold standard segmentation mask of LV, MYO and RV Zhuang and Shen (2016); Wu and Zhuang (2020). For experiments, we use the 16 slices from each 3D image. These 2D slices were extracted from the long-axis view around the center of left ventricular cavity Wu and Zhuang (2020). Specifically, 320 labeled and 512 unlabeled slices are from CT images, while 320 labeled and 416 unlabeled slices are from MR images.

To evaluate the generalization of DS²Net, we follow Pei et al. (2021) and conduct cross-domain experiments (5-Fold cross-validation) including adaptation from CT images to MR image and adaptation from MR images to CT image. The segmentation results (Dice metric) and visualization results are respectively shown in Tab.9 and Fig.11. Here,

¹https://github.com/FupingWu90/CT_MR_2D_Dataset_DA

Table 9

Segmentation experiments on bidirectional CT-MR unsupervised domain adaptation. All methods are evaluated with Dice metric (%). † indicates results reported from Pei et al. (2021).

CT → MR				
Methods	MYO	RV	LV	Mean
PSPNet (supervised) Zhao et al. (2017)	78.1±3.2	85.7±2.5	91.0±2.8	84.9±3.0
SegFormer (supervised) Xie et al. (2021)	84.3±4.1	90.7±3.2	92.6±3.8	89.2±4.1
PSPNet (w/o DA) Zhao et al. (2017)	24.6±3.2	57.1±3.5	66.4±3.8	49.4±3.5
SegFormer (w/o DA) Xie et al. (2021)	40.8±4.6	68.1±4.0	73.9±4.8	60.9±4.9
CycleSeg† Zhu et al. (2017)	53.2±17.1	79.2±13.1	81.3±11.8	71.2±19.1
EGUDA_T Zeng et al. (2020)	64.7±5.5	76.4±4.2	80.5±4.6	73.9±5.0
DAFormer Hoyer et al. (2022)	66.4±3.7	82.8±4.9	85.0±4.4	78.1±4.5
SIFA† Chen et al. (2020)	67.3±11.4	84.2±11.5	87.6±8.9	79.6±13.9
DDFSeg† Pei et al. (2021)	71.3±10.6	83.2±11.7	87.7±10.4	80.7±12.9
EDRL Wang et al. (2023)	75.6±6.9	87.1±4.7	91.6±5.7	84.8±4.1
DS ² Net_P	63.5±4.0	74.3±3.7	80.4±4.4	72.7±4.3
DS ² Net_T	70.2±4.3	82.5±5.0	87.0±4.1	79.9±5.1
MR → CT				
PSPNet (supervised) Zhao et al. (2017)	80.9±2.8	86.1±3.0	89.6±2.5	85.5±3.0
SegFormer (supervised) Xie et al. (2021)	88.4±3.2	92.1±3.2	93.3±3.8	91.3±3.5
PSPNet (w/o DA) Zhao et al. (2017)	27.8±2.2	48.8±2.9	58.3±2.4	45.0±2.8
SegFormer (w/o DA) Xie et al. (2021)	38.1±4.6	65.4±4.3	74.0±3.8	59.1±4.4
EGUDA_T Zeng et al. (2020)	52.2±6.3	77.4±4.3	81.9±5.2	70.5±5.7
CycleSeg† Zhu et al. (2017)	51.3±15.4	83.3±7.7	79.3±15.3	71.3±19.5
SIFA† Chen et al. (2020)	56.6±12.4	80.0±8.3	82.6±12.6	73.1±16.3
DAFormer Hoyer et al. (2022)	61.8±5.1	78.3±3.2	81.7±4.9	73.9±5.4
DDFSeg† Pei et al. (2021)	66.9±11.0	79.1±6.7	83.5±16.0	76.5±13.8
EDRL Wang et al. (2023)	77.1±11.1	87.0±9.1	87.4±16.6	84.0±10.3
DS ² Net_P	53.6±4.7	72.0±4.2	82.3±5.0	69.3±4.9
DS ² Net_T	65.4±5.7	78.6±4.6	85.7±5.8	76.6±6.0

we’d like to analyze in the following points. (1) Compared to DDFSeg, DS²Net_T achieves comparable results. On “CT → MR” UDA segmentation task, DS²Net_T has little inferiority than DDFSeg (0.8% less in Dice metric). On “MR → CT” UDA segmentation task, DS²Net_T outperforms DDFSeg by 0.1% in Dice metric. (2) Obviously, EDRL is the current SOTA methods. Even though DS²Net is inferior to EDRL, the second-best results can still prove its generalization capability. (3) Obviously, DS²Net has less standard deviation than previous methods. The main reason is that CycleSeg, SIFA, DDFSeg and EDRL all adopt pixel-to-pixel image translation for alignment. Compared to image alignment mechanism, feature alignment mechanism is more stable during optimization. Our proposed DS²Net is a typical feature alignment based method, which leads to low-fluctuation among different runs. (4) Compared to OTU_2d/OTU_CEUS, CT/MR images obviously have larger domain shift. In this case, image alignment based methods have more advantages. (5) In Fig.11, we provide 4 cases to visualize the segmentation prediction on bidirectional CT-MR unsupervised domain adaptation. This visualization coincides with results shown in Tab.9. As a whole, experimental results on CT/MR (MM-WHS) UDA semantic segmentation task prove the generalization of DS²Net.

5.3. Single-Modality Recognition

On Task1 and Task2, we apply a “foreground-background” lesion area segmentation without directly applying seven/eight-category segmentation. Therefore, we tackle single-modality

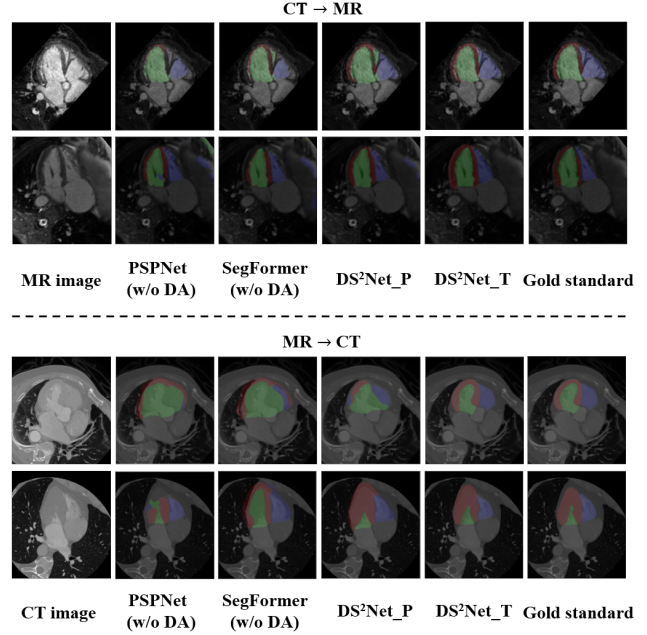


Figure 11: Visualization of segmentation results on bidirectional CT-MR unsupervised domain adaptation. The region of MYO, RV and LV are respectively indicated by red, blue and green. Here, electronic version are recommended for readers.

Table 10

Single-modality recognition results on MMOTU image dataset. We adopt top1 and top2 accuracy as our metric.

Methods	OTU_2d		OTU_CEUS	
	top1 (%)	top2 (%)	top1 (%)	top2 (%)
VGG-16	67.59	79.96	61.0	74.0
ResNet-34	77.61	88.70	69.0	79.0
ResNet-50	80.17	90.19	72.0	81.0
DenseNet-121	78.89	89.34	69.0	77.0
MobileNetV2	76.97	86.78	68.0	78.0
EfficientNet-b0	76.12	85.93	64.0	79.0
EfficientNet-b1	77.61	86.99	71.0	79.0
EfficientNetV2-S	79.74	89.55	70.0	80.0
EfficientNetV2-M	80.60	91.04	71.0	81.0

image recognition in Task3 (Fig.1) to classify ovarian tumors. In this paper, we provide VGG Simonyan and Zisserman (2015), ResNet He et al. (2016), DenseNet Huang et al. (2017), EfficientNet Tan and Le (2019a), MobileNetV2 Sandler et al. (2018) and EfficientNetV2 Tan and Le (2019b) as baseline classification models. For all models, we select SGD as optimizer. The momentum and weight decay value are set as 0.9 and 0.0005. All model are loaded ImageNet-pretrained weights before training. As shown in Tab.10, EfficientNetV2-M outperforms other methods on OTU_2d while ResNet-50 achieves close results. On OTU_CEUS, ResNet-50 outperforms other methods while EfficientNet-b1 and EfficientNetV2-M achieve close results. Generally,

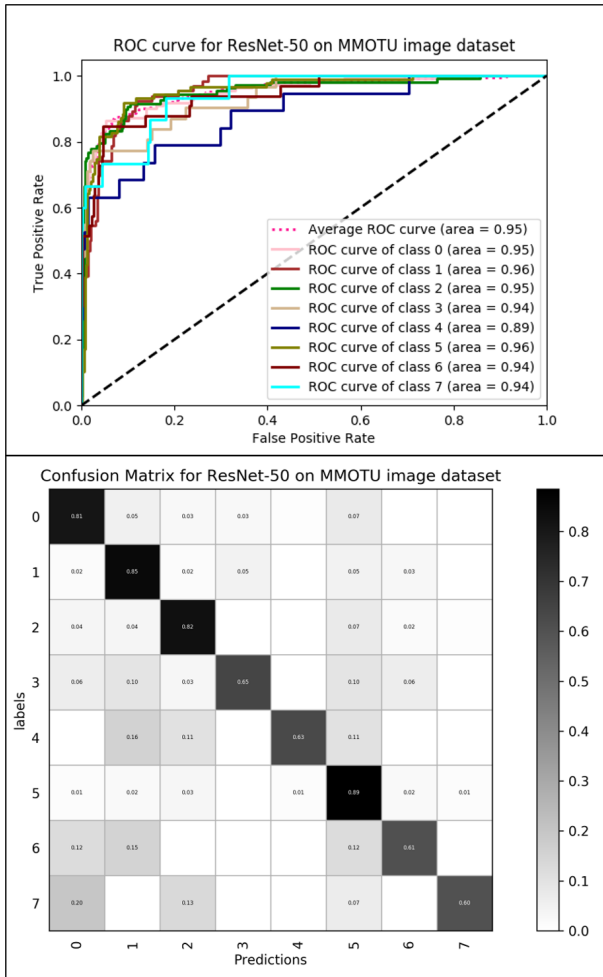


Figure 12: ROC curve and confusion matrix on 8 ovarian tumor categories. Here, we conduct experiments on OTU_2d and select ResNet-50 as classification network.

ResNet-50 and EfficientNetV2 show strong generalization capability on single-modality recognition task. Moreover, besides top1 accuracy, we also use top2 accuracy as metric because providing two category candidates is also valuable for diagnosis in practical medical treatment.

To better present the single-modality recognition performance, we select ResNet-50 as classification network and further evaluate it with ROC curve and confusion matrix on OTU_2d. Obviously, experiments results from classification accuracy (Tab.10), AUC (area under curve) and confusion matrix are mutually corroborated. We also find that the Chocolate cyst, Serous cystadenoma, Teratoma and Normal ovary (category 0, 1, 2, 5) obviously have better classification accuracy than Theca cell tumor, Simple cyst, Mucinous cystadenoma and High grade serous (category 3, 4, 6, 7). The main reason is that “category 0, 1, 2, 5” have more training samples the “category 3, 4, 6, 7” (Fig.2).

5.4. Discussion

In this paper, we propose MMOTU image dataset containing 2d ultrasound and CEUS images. Based on our

proposed dataset, we tackle three tasks and mainly focus on bidirectional UDA segmentation between 2d ultrasound and CEUS images. To boost the cross-domain segmentation performance, we propose DS²Net, which works well on closing the representation gap between 2d ultrasound and CEUS images. Our research provides an insight on detecting ovarian tumors on multi-modality ultrasound images, especially on CEUS images. Our research can also be regarded as an AI-aided technique for clinical diagnosis and treatment.

5.4.1. Discussion on the Risk of Model Biasing by Symbols on Images

As mentioned in Fig.3, there are some symbols on images. Due to historical and practical reasons, we can not collect pure raw data. Naturally, there may raise a question, is there a risk of biasing the model by symbols during optimization? In this section, we conduct experiments on single-modality 2d ultrasound image segmentation and cross-domain segmentation tasks to analyze the influence of symbols.

To remove the symbols from images, we apply the recent notable image inpainting method Yu et al. (2019) on all samples in MMOTU image dataset. Then we use the original and “symbol-free” MMOTU image dataset to respectively train models. We will discuss the results shown in Tab.11 as follows. (1) Generally, models trained with “symbol-free” samples show performance decline. (2) This comparison is a little bit unreasonable because the training and testing set both changes after removing the symbols. However, we can still roughly draw a conclusion that applying image inpainting technique is not necessary. (3) Intuitively, images after removing symbols are not becoming distorted or destroyed. However, it also change the data in an implicit manner. It means that the negative influence from data distribution change outweighs the positive influence from symbol interference. (4) From another perspective, experts are not confused by those symbols during annotating the images, which means the symbols have little impact on visual features of images. Therefore, we believe that our models can also overcome the interference of symbols and learn those important and useful features.

As a whole, symbols on images may harm segmentation performance, but we find the harm is limited from the experiments. Moreover, inpainting on MMOTU image dataset is not recommended. It’d be better to preserve raw data.

5.4.2. Limitations and Future Works

However, our research still has some limitations to be improved. Here, we summarize four main limitations as follows. (1) As shown in Fig.3, some symbols are left on our collected images. Due to some historical and practical reasons, we can not collect pure raw data without symbols, which may cause model biasing by symbols during optimization. (2) MMOTU image dataset has only 170 CEUS images. Lacking both training and testing images will harm the credibility of experiments. (3) DS²Net shows strong performance on CEUS images (single-frame) trained with

Table 11

Semantic segmentation results comparison between models trained by images with and w/o symbols. On single-modality segmentation, we select PSPNet and SegFormer as example.

Single-modality segmentation results on MMOTU image dataset				
Methods	OTU_2d		OTU_CEUS	
	IoU(%)	mIoU(%)	IoU(%)	mIoU(%)
PSPNet	82.01	89.41	71.01	81.6
PSPNet (w/o symbols)	81.13	88.63	70.78	81.09
SegFormer	82.46	89.88	73.03	83.0
SegFormer (w/o symbols)	81.52	89.17	72.62	82.55
UDA segmentation results on MMOTU image dataset				
Methods	OTU_CEUS → OTU_2d		OTU_2d → OTU_CEUS	
	IoU(%)	mIoU(%)	IoU(%)	mIoU(%)
DS ² Net_P	54.06	71.87	61.85	75.75
DS ² Net_P (w/o symbols)	52.93	70.46	60.49	74.62
DS ² Net_T	65.42	79.20	69.81	80.86
DS ² Net_T (w/o symbols)	64.03	78.02	68.58	79.43

2d ultrasound images. However, DS²Net can not directly apply on CEUS sequences, which means there still exists challenges to spread our proposed AI-aided technique on clinical CEUS examination. (4) Our paper lacks of detailed analysis on recognition task (Task3, Fig.1). Although we mainly focus on lesion segmentation, recognition of tumor type is also a meaningful task in practical clinical diagnosis.

In the future, we will further extend our work and focus in the following aspects. (1) We will continually extend our proposed MMOTU image dataset, especially OTU_CEUS. We will also pay attention to preserving pure data without symbols. (2) Actually, the total tumor categories of OTU_2d are 32. Since some of tumor types (e.g. fibrosarcoma) have only one or two samples, we exclude them in our dataset. In the future, we will extend the categories together with collecting more data. (3) In MMOTU image dataset, samples of each category are unbalanced. We will further explore its influence. (4) In this work, we explore the AI-aided techniques on CEUS images. In the future, we will further explore the AI-aided methods on CEUS sequences, which is more valuable and meaningful. (5) We will try to migrate our method on other cross-modality data (e.g., CT/MRI) for cross-domain adaptation segmentation task to prove the robustness of our method.

6. Conclusion

In this paper, we propose a multi-modality ovarian tumor ultrasound (MMOTU) image dataset to explore the cross-domain representation potential. MMOTU image dataset contains 1469 2d ultrasound images and 170 CEUS images with pixel-wise and global-wise annotations. Based on MMOTU image dataset, we mainly focus on alleviating the domain shift problem on lesion area segmentation for bidirectional unsupervised domain adaptation between 2d ultrasound and CEUS images. In this paper, we propose DS²Net, which is a feature alignment based architecture. Specifically, we use adversarial learning to first ease the

domain shift of encoders for better representation on both source and target images. Then, we design DDSM and DUSM to extract the domain-distinct and domain universal features. With these two modules, each encoder and decoder-head will further have specific style feature representation capability towards both source and target images. Extensive experiments show that the DS²Net outperforms the previous notable feature alignment based methods on MMOTU image dataset. Visualization and analysis also prove that DS²Net is convincing and interpretable. In this paper, we also provide series of baseline models on single-modality semantic segmentation and recognition tasks. Compared to previous methods, we first propose method to tackle the cross-domain ovarian tumor segmentation on our proposed MMOTU image dataset, which provides a new insight on detecting ovarian tumors.

CRedit Author Statement

Qi Zhao: Conceptualization, Supervision, Project administration. **Shuchang Lyu:** Conceptualization, Methodology, Software, Writing - Original Draft. **Wenpei Bai:** Validation, Writing - Review & Editing, Funding acquisition. **Linghan Cai:** Data Curation, Formal analysis. **Binghao Liu:** Validation, Visualization. **Guangliang Cheng:** Supervision, Writing - Review & Editing. **Meijing Wu:** Data Curation. **Xiubo Sang:** Data Curation. **Min Yang:** Resources. **Lijiang Chen:** Investigation, Writing - Review & Editing.

Acknowledgment

All the data collected in our proposed dataset have appropriate approvals from the ethics committees of Beijing Shijitan Hospital, Capital Medical University. This work was supported by the National Natural Science Foundation of China (grant numbers 62072021).

References

- Biase, A.D., Tang, W., Sourlos, N., et al., 2021. Skip-sece multi-scale attention and co-learning method for oropharyngeal tumor segmentation on multi-modal PET-CT images, in: HECKTOR 2021, Held in Conjunction with MICCAI 2021, pp. 109–120.
- Cao, H., Wang, Y., Chen, J., et al., 2021. Swin-unet: Unet-like pure transformer for medical image segmentation. CoRR abs/2105.05537.
- Chartsias, A., Papanastasiou, G., Wang, C., et al., 2021. Disentangle, align and fuse for multimodal and semi-supervised image segmentation. IEEE Trans. Medical Imaging 40, 781–792.
- Chen, C., Dou, Q., Chen, H., et al., 2020. Unsupervised bidirectional cross-modality adaptation via deeply synergistic image and feature alignment for medical image segmentation. IEEE Trans. Medical Imaging 39, 2494–2505.
- Chen, C., Dou, Q., Jin, Y., et al., 2019a. Robust multimodal brain tumor segmentation via feature disentanglement and gated fusion, in: Medical Image Computing and Computer Assisted Intervention, pp. 447–456.
- Chen, J., Lu, Y., Yu, Q., et al., 2021. Transunet: Transformers make strong encoders for medical image segmentation. CoRR abs/2102.04306. URL: <https://arxiv.org/abs/2102.04306>.
- Chen, X., Zhang, R., Yan, P., 2019b. Feature fusion encoder decoder network for automatic liver lesion segmentation, in: International Symposium on Biomedical Imaging, pp. 430–433.

- Chi, J., Walia, E., Babyn, P.S., et al., 2017. Thyroid nodule classification in ultrasound images by fine-tuning deep convolutional neural network. *J. Digit. Imaging* 30, 477–486.
- Deng, J., Dong, W., Socher, R., et al., 2009. Imagenet: A large-scale hierarchical image database, in: *IEEE Conference on Computer Vision and Pattern Recognition*, pp. 248–255.
- Dosovitskiy, A., Beyer, L., Kolesnikov, A., et al., 2021. An image is worth 16x16 words: Transformers for image recognition at scale, in: *International Conference on Learning Representations*.
- Dou, Q., Ouyang, C., Chen, C., et al., 2019. Pnp-adanet: Plug-and-play adversarial domain adaptation network at unpaired cross-modality cardiac segmentation. *IEEE Access* 7, 99065–99076.
- Du, L., Tan, J., Yang, H., et al., 2019. SSF-DAN: separated semantic feature based domain adaptation network for semantic segmentation, in: *IEEE International Conference on Computer Vision*, pp. 982–991.
- Fu, J., Liu, J., Tian, H., et al., 2019. Dual attention network for scene segmentation, in: *IEEE Conference on Computer Vision and Pattern Recognition*, pp. 3146–3154.
- He, K., Zhang, X., Ren, S., Sun, J., 2016. Deep residual learning for image recognition, in: *IEEE Conference on Computer Vision and Pattern Recognition*, pp. 770–778.
- He, X., Deng, Y., Fang, L., Peng, Q., 2021. Multi-modal retinal image classification with modality-specific attention network. *IEEE Trans. Medical Imaging* 40, 1591–1602.
- Hoffman, J., Tzeng, E., Park, T., et al., 2018. Cycada: Cycle-consistent adversarial domain adaptation, in: *International Conference on Machine Learning*, pp. 1994–2003.
- Hoyer, L., Dai, D., Gool, L.V., 2022. Daformer: Improving network architectures and training strategies for domain-adaptive semantic segmentation, in: *IEEE Conference on Computer Vision and Pattern Recognition*, IEEE. pp. 9914–9925.
- Huang, G., Liu, Z., van der Maaten, L., et al., 2017. Densely connected convolutional networks, in: *IEEE Conference on Computer Vision and Pattern Recognition*, pp. 2261–2269.
- Isola, P., Zhu, J., Zhou, T., et al., 2017. Image-to-image translation with conditional adversarial networks, in: *IEEE Conference on Computer Vision and Pattern Recognition*, pp. 5967–5976.
- Kaul, C., Manandhar, S., Pears, N.E., 2019. Focusnet: An attention-based fully convolutional network for medical image segmentation, in: *International Symposium on Biomedical Imaging*, pp. 455–458.
- Li, D., Peng, Y., Sun, J., et al., 2023. Unsupervised deep consistency learning adaptation network for cardiac cross-modality structural segmentation. *Medical & biological engineering & computing*.
- Li, H., Fang, J., Liu, S., et al., 2020. Cr-unet: A composite network for ovary and follicle segmentation in ultrasound images. *IEEE J. Biomed. Health Informatics* 24, 974–983.
- Li, S., Sui, X., Luo, X., et al., 2021. Medical image segmentation using squeeze-and-expansion transformers, in: *International Joint Conference on Artificial Intelligence*, pp. 807–815.
- Liang, Z., Zhao, K., Liang, G., et al., 2023. Maxformer: Enhanced transformer for medical image segmentation with multi-attention and multi-scale features fusion. *Knowledge-Based Systems* 280, 110987.
- Liu, Z., Lin, Y., Cao, Y., et al., 2021. Swin transformer: Hierarchical vision transformer using shifted windows, in: *IEEE International Conference on Computer Vision*, pp. 9992–10002.
- Mathur, P., Kakwani, K., Diplav, et al., 2020. Deep learning based quantification of ovary and follicles using 3d transvaginal ultrasound in assisted reproduction, in: *International Conference of the Engineering in Medicine & Biology Society*, pp. 2109–2112.
- Narra, R.T., Singhal, N., Narayan, N.S., et al., 2018. Automated ovarian volume quantification in transvaginal ultrasound, in: *International Symposium on Biomedical Imaging*, pp. 1513–1516.
- Oktay, O., Schlemper, J., Folgoc, L.L., et al., 2018. Attention u-net: Learning where to look for the pancreas. *CoRR abs/1804.03999*.
- Ouyang, C., Kamnitsas, K., Biffi, C., et al., 2019. Data efficient unsupervised domain adaptation for cross-modality image segmentation, in: *Medical Image Computing and Computer Assisted Intervention*, pp. 669–677.
- Paschali, M., Gasperini, S., et al., 2019. 3dq: Compact quantized neural networks for volumetric whole brain segmentation, in: *Medical Image Computing and Computer Assisted Intervention*, pp. 438–446.
- Pei, C., Wu, F., Huang, L., et al., 2021. Disentangle domain features for cross-modality cardiac image segmentation. *Medical Image Anal.* 71, 102078.
- Qian, J., Li, R., Yang, X., et al., 2022. HASA: hybrid architecture search with aggregation strategy for echinococcosis classification and ovary segmentation in ultrasound images. *CoRR abs/2204.06697*.
- Ronneberger, O., Fischer, P., Brox, T., 2015. U-net: Convolutional networks for biomedical image segmentation, in: *Medical Image Computing and Computer-Assisted Intervention*, pp. 234–241.
- Sandler, M., Howard, A.G., Zhu, M., et al., 2018. Mobilenetv2: Inverted residuals and linear bottlenecks, in: *IEEE Conference on Computer Vision and Pattern Recognition*, pp. 4510–4520.
- Siegel, R.L., Miller, K.D., Fuchs, H.E., et al., 2021. *Cancer statistics, 2021*. CA: A Cancer Journal for Clinicians 71.
- Simonyan, K., Zisserman, A., 2015. Very deep convolutional networks for large-scale image recognition, in: *International Conference on Learning Representations*.
- Tan, M., Le, Q.V., 2019a. Efficientnet: Rethinking model scaling for convolutional neural networks, in: *International Conference on Machine Learning*, pp. 6105–6114.
- Tan, M., Le, Q.V., 2019b. Efficientnetv2: Smaller models and faster training, in: *International Conference on Machine Learning*, pp. 6105–6114.
- Tsai, Y., Hung, W., Schuler, S., et al., 2018. Learning to adapt structured output space for semantic segmentation, in: *IEEE Conference on Computer Vision and Pattern Recognition*, pp. 7472–7481.
- Valindria, V.V., Pawlowski, N., Rajchl, M., et al., 2018. Multi-modal learning from unpaired images: Application to multi-organ segmentation in CT and MRI, in: *IEEE Winter Conference on Applications of Computer Vision*, pp. 547–556.
- Wanderley, D.S., Carvalho, C.B., Domingues, A., et al., 2018. End-to-end ovarian structures segmentation, in: *Progress in Pattern Recognition, Image Analysis, Computer Vision and Applications*, pp. 681–689.
- Wang, H., Liu, C., Zhao, Z., et al., 2021. Application of deep convolutional neural networks for discriminating benign, borderline, and malignant serous ovarian tumors from ultrasound images. *Frontiers in Oncology* 11.
- Wang, R., Zhou, Q., Zheng, G., 2023. Edrl: Entropy-guided disentangled representation learning for unsupervised domain adaptation in semantic segmentation. *Computer methods and programs in biomedicine* 240, 107729.
- Wang, S., Yu, L., Yang, X., et al., 2019. Patch-based output space adversarial learning for joint optic disc and cup segmentation. *IEEE Trans. Medical Imaging* 38, 2485–2495.
- Wang, Y., Zeng, Q., 2021. Ovarian tumor texture classification based on sparse auto-encoder network combined with multi-feature fusion and random forest in ultrasound image. *J. Medical Imaging Health Informatics* 11, 424–431.
- Wang, Z., Zou, N., Shen, D., et al., 2020. Non-local u-nets for biomedical image segmentation, in: *AAAI Conference on Artificial Intelligence*, pp. 6315–6322.
- Wu, C., Wang, Y., Wang, F., 2018. Deep learning for ovarian tumor classification with ultrasound images, in: *Advances in Multimedia Information Processing PCM*, pp. 395–406.
- Wu, F., Zhuang, X., 2020. CF distance: A new domain discrepancy metric and application to explicit domain adaptation for cross-modality cardiac image segmentation. *IEEE Trans. Medical Imaging* 39, 4274–4285.
- Wu, X., Feng, Y., Xu, H., Lin, Z., Chen, T., Li, S., Qiu, S., Liu, Q., Ma, Y., Zhang, S., 2023. Ctranscn: Combining transformer and cnn in multilabel medical image classification. *Knowledge-Based Systems* 281, 111030.
- Xie, E., Wang, W., Yu, Z., et al., 2021. Segformer: Simple and efficient design for semantic segmentation with transformers, in: *Advances in Neural Information Processing Systems*, pp. 12077–12090.

- Yang, J., Dvornek, N.C., Zhang, F., et al., . Unsupervised domain adaptation via disentangled representations: Application to cross-modality liver segmentation, in: Medical Image Computing and Computer Assisted Intervention, pp. 255–263.
- Yang, S., Zhang, X., Chen, Y., et al., 2023. Ucnunet: A lightweight and precise medical image segmentation network based on efficient large kernel u-shaped convolutional module design. Knowledge-Based Systems 278, 110868.
- Yang, X., Li, H., Wang, Y., et al., 2021. Contrastive rendering with semi-supervised learning for ovary and follicle segmentation from 3d ultrasound. Medical Image Anal. 73, 102134.
- Yu, C., Gao, C., Wang, J., et al., 2021. Bisenet V2: bilateral network with guided aggregation for real-time semantic segmentation. Int. J. Comput. Vis. 129, 3051–3068.
- Yu, J., Lin, Z., Yang, J., et al., 2019. Free-form image inpainting with gated convolution, in: IEEE International Conference on Computer Vision, pp. 4471–4480.
- Zeng, G., Lerch, T.D., Schmaranzer, F., et al., 2021. Semantic consistent unsupervised domain adaptation for cross-modality medical image segmentation, in: Medical Image Computing and Computer Assisted Intervention, pp. 201–210.
- Zeng, G., Schmaranzer, F., Lerch, T.D., et al., 2020. Entropy guided unsupervised domain adaptation for cross-center hip cartilage segmentation from MRI, in: Medical Image Computing and Computer Assisted Intervention, pp. 447–456.
- Zhan, B., Song, E., et al., 2023. Segmenting medical images via explicit–implicit attention aggregation. Knowledge-Based Systems 279, 110932.
- Zhang, Y., Chen, H., Wei, Y., et al., 2019. From whole slide imaging to microscopy: Deep microscopy adaptation network for histopathology cancer image classification, in: Medical Image Computing and Computer Assisted Intervention, pp. 360–368.
- Zhang, Y., Liu, H., Hu, Q., 2021. Transfuse: Fusing transformers and cnns for medical image segmentation, in: Medical Image Computing and Computer Assisted Intervention, pp. 14–24.
- Zhao, H., Shi, J., Qi, X., et al., 2017. Pyramid scene parsing network, in: IEEE Conference on Computer Vision and Pattern Recognition, pp. 6230–6239.
- Zhou, Z., Siddiquee, M.M.R., Tajbakhsh, N., Liang, J., 2018. Unet++: A nested u-net architecture for medical image segmentation, in: Deep Learning in Medical Image Analysis - and - Multimodal Learning for Clinical Decision Support, pp. 3–11.
- Zhu, J., Park, T., Isola, P., et al., 2017. Unpaired image-to-image translation using cycle-consistent adversarial networks, in: IEEE International Conference on Computer Vision, pp. 2242–2251.
- Zhu, M., Chen, Z., Yuan, Y., 2021. Dsi-net: Deep synergistic interaction network for joint classification and segmentation with endoscope images. IEEE Trans. Medical Imaging 40, 3315–3325.
- Zhuang, X., Shen, J., 2016. Multi-scale patch and multi-modality atlases for whole heart segmentation of MRI. Medical Image Anal. 31, 77–87.
- Zou, D., Zhu, Q., Yan, P., 2020. Unsupervised domain adaptation with dual-scheme fusion network for medical image segmentation, in: International Joint Conference on Artificial Intelligence, pp. 3291–3298.